FLITECAM

Handbook for Archive Users

J. De Buizer, W. Reach

Rev 1.0
Date: 2023 Dec 14

REVISIONS

REV	DATE	DESCRIPTION
0.0	2023/10/04	Initial draft
0.1	2023/11/13	First full draft
0.2	2023/12/01	Major updates
0.3	2023/12/05	Content complete; final formatting applied
1.0	2023/12/14	Final copyediting applied; Released as Version 1.0.

FLITECAM Handbook for Archive Users

Table of Contents

1. ESSENTIAL INFORMATION

Table 1: General Information About FLITECAM

Instrument wavelength total range[1]	1.0 < λ < 5.5 μm
Detector Type [2]	InSb Raytheon ALADDIN III
Pixel size[1]	0.475 arcsec
Array size[1]	1024 × 1024 pixels
Field of view[3]	5.6 arcmin diameter[3]
Main observing modes[4]	Imaging, Long Slit Grism Spectroscopy[4]
Spectroscopy slit widths[1]	1.0 and 2.0 arcsec
SOFIA observing cycles in service	Cycle 1 to Cycle 6[5]
Years in service	2013 to 2018
Built by	UCLA (PI: Ian McLean)

[1]See Section 2.1 for an in-depth overview of FLITECAM's technical specifications; [2]For more information on the detector properties, see Section 2.2; [3]Actual FOV was ~8′, but because of coma at the edges and the inclusion of a field stop the effective size of the field was restricted to 5.6′ (see Section 3.7); [4]See Section 2.3. [5]FLITECAM was offered for Cycle 6 but took no science data in that cycle.

Table 2: Imaging Filters, Effective Wavelengths and Bandwidth

Bandpass	Filter Name	λ_{eff} [a] (μm)	5% Bandwidth[b] (μm)	Spatial Resolution[c] (FWHM in ″)
Standard Filters				
J	FLT_J	1.24	0.29	3.4±0.2
H	FLT_H	1.63	0.31	3.3±0.1
K	FLT_K	2.10	0.40	3.0±0.1
L	FLT_L	3.53	0.65	-[d]
L′	FLT_Lprime	3.86	0.70	-[d]
M	FLT_M	4.84	0.65	-[d]
Specialty Filters				
Paschen α	FLT_Pa	1.87	0.03	3.3±0.2
Pa α Continuum	FLT_Pa_Cont	1.90	0.03	3.0±0.1
H_2O Ice	FLT_ICE_308	3.05	0.19	2.8±0.1
PAH	FLT_PAH_329	3.30	0.12	2.8±0.2
L_{narrow}	FLT_NbL	3.61	0.23	2.7±0.3

M_{narrow}	FLT_NbM	4.80	0.19	-[d]
Order Sorting Filters				
H_{wide}	Hwide	1.79	0.59	-
K_{wide}	Kwide	2.30	0.88	-
K_{long}	Klong	2.45	0.55	-
L+M	L+M	4.11	2.72	-

[a]Mean and pivot wavelengths for all FLITECAM filters are given in Table 12, and depend on whether the instrument was in the FLITECAM-only or FLIPO configuration. [b]Bandwidth for transmission level is >5%. [c]These image quality measurements are from FLITECAM commissioning flights in 2014 only, and L and M bands were not tested. [d]L, L', M and M_{narrow} were not fully characterized and never used for science.

Table 3: Spectroscopic Grism Characteristics, Wavelength Range, Spectral Resolution

Name[a]	Grism	Order	Order Sorting Filters	Wavelength Range (μm)	R (λ/Δλ)	
					High- Res[b]	Low-Res[b]
FLT_A1_LM	**A**	1[c]	L+M[c]	4.395–5.533[c]	—[c]	—[c]
FLT_A2_KL		2	K_{long}	2.270–2.722	1690	1140
FLT_A3_Hw		3	H_{wide}	1.550–1.828	1710	1290
FLT_B1_LM	**B**	1[c]	L+M[c]	3.303–4.074[c]	1780[c]	1200[c]
FLT_B2_Hw		2	H_{wide}	1.675–2.053	1750	1320
FLT_B3_J		3	J	1.140–1.385	1720	1425
FLT_C2_LM	**C**	2	L+M	2.779–3.399	1670	1300
FLT_C3_Kw		3	K_{wide}	1.910–2.276	1650	1390
FLT_C4_H		4	H	1.500–1.718	1640	1400

[a] These are the names of these observational setups as given in the FLITECAM headers and defined as the "spectral element" when searching for data with the IRSA archive.

[b] There are two slits used for spectroscopy which are both 60" long. The 'narrow' slit is 1" wide and provides 'high' resolution spectroscopy, while the 'wide' slit is 2" wide and provides 'low' resolution spectroscopy. Since the two resolutions are similar, when searching for FLITECAM data using the IRSA archive there is only one resolution option given: "Medium Resolution Spectroscopy (R~1000)".

[c] This combination of grism and order sorting filter was not fully characterized and was offered only for a short time on a shared risk (experimental) basis.

2. INSTRUMENT DESCRIPTION

In this section the design and observing modes of the FLITECAM instrument are discussed. For information about the scientific objectives of FLITECAM and its unique capabilities, see the introduction to Section 5.

2.1 FLITECAM OVERVIEW

The First Light Infrared TEst CAMera (FLITECAM) was an infrared camera, operating in the 1.0 - 5.5 μm range. It had a set of broadband filters for imaging, and a set of grisms and order sorting filters for medium resolution spectroscopy. The FLITECAM imaging mode provided seeing-limited images at 1 – 3 μm and diffraction-limited images at 3 - 5.5 μm (McLean et al. 2006). The detector was an indium antimonide (InSb) Raytheon ALADDIN III array that was 1024 × 1024 pixels in size with a pixel scale of 0.475″ per pixel. This configuration resulted in a field-of-view (FOV) of ~8.0′ but a circular stop and coma at the edges of the image restricted the usable FOV to 5.6′ (see Section 3.7). FLITECAM had two filter wheels that contained a set of broadband imaging filters, a suite of broad order sorting filters for spectroscopy, and a few narrowband-imaging filters (see Table 3). Available broadband imaging filters for FLITECAM were J, H, K, L, L′, and M. The narrow band filters were L_{narrow}, M_{narrow}, Paschen Alpha (1.87 μm), Paschen Alpha Continuum (at 1.90 μm), a filter covering the water ice band at 3.05 μm, and another covering the 3.30 μm PAH band. It should be noted that the broadband filters (J, H, K, L, L′, and M) were specifically designed for observations at SOFIA altitudes and were not necessarily the same as those found at ground-based observatories (e.g., 2MASS).

FLITECAM also had three grisms and five order-sorting filters (OSFs) that could be combined in different ways in order to access the full 1.0 - 5.5 μm wavelength range. It had two slit withs available, a narrow slit (1″) and a wide slit (2″), which allowed for higher (R~1700) or lower resolution (R~1300), respectively. Grisms were chosen for use in FLITECAM since they minimized the changes necessary to the optical path while still allowing moderate spectral resolution observations. The grisms were made of direct-ruled (i.e., etched) KRS-5 (thallium bromoiodide) material that provided a relatively high index of refraction (n ~ 2.4) without the significant absorption features that plague grisms with adhered transmission gratings. The three grisms were fabricated by Carl-Zeiss (Jena, Germany) each with an apex angle of 34.4°, but with different groove spacings to allow coverage of the entire 1–5.5 μm band.

Though it was originally slated to be the first-light camera for SOFIA (as its name suggests), the name had become a misnomer when (for various reasons) the FORCAST instrument was instead chosen to help commission the observatory and provide first light in 2010. One unique aspect of FLITECAM was that it could be co-mounted with the High-speed Imaging Photometer for Occultations (HIPO) providing simultaneous optical and near-infrared imaging for transient events. FLITECAM was in operation from 2013-2018 (Cycles 1-6), before being decommissioned by NASA in 2018. Since the main focus of SOFIA was longer wavelength infrared observations, during its operating lifetime FLITECAM observed only a modest total number of science targets. A list of these targets is given in Appendix A.

2.2 INSTRUMENT DESIGN

FLITECAM consisted of a cryogenically cooled near-IR (NIR) camera that could be used for both imaging and grism spectroscopy. A schematic of the optical bench is shown in Figure 1 with a full ray trace diagram in Figure 2.

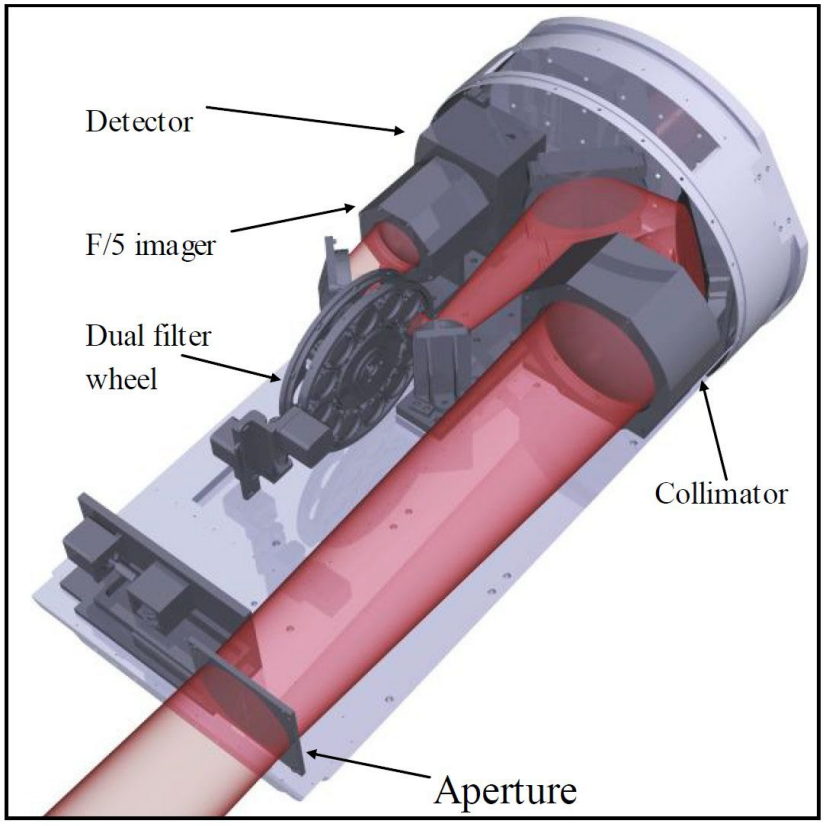

Figure 1 *This is a block diagram of the front end of the FLITECAM instrument with labels of important components. In red is the light path through the instrument optics (see Figure 2 for more details).*

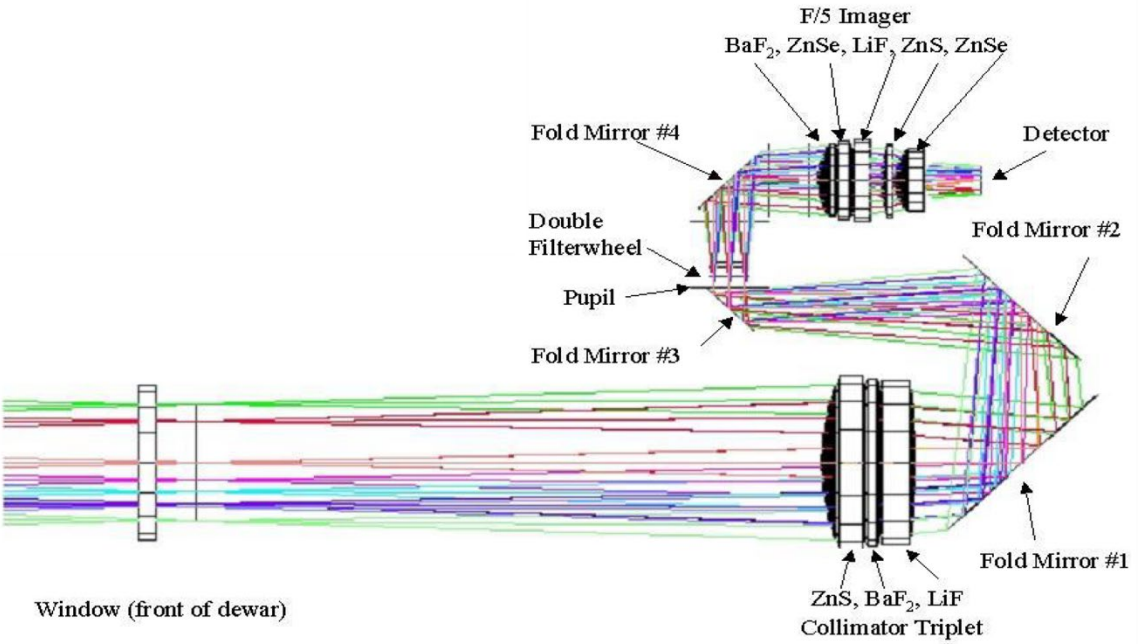

Figure 2 *The FLITECAM ray trace diagram with all optical elements labeled.*

The incoming beam first passed through the entrance aperture and into the collimator assembly, a stack of custom designed lenses that allowed imaging of nearly the entire 8' × 8' SOFIA observatory field of view (FOV). The beam was then repositioned using three flat fold-mirrors so that it passed through the image pupil and through a pair of 12-position filter wheels. A fourth flat fold mirror redirected the beam through the f/4.7 refractive imaging assembly, which then focused the beam on the array.

When observing in spectroscopy mode, only minimal changes to the optical path were required. First, the slit mask was inserted into the beam immediately behind the aperture window at the telescope focus. The slit was a single 16.5 mm long slit (2′ on the detector) divided in half with two different widths, one approximately 2″ and the other 1″. Second, the chosen grism and order sorting filter (located in filter wheel #2 and #1, respectively) were set in place.

The FLITECAM detector was cryogenically cooled to 30 K, yielding read noise of approximately 40 e and dark current ≤ 1 e/sec. The detector well depth was relatively shallow (~ 80,000 e) which, when combined with the detector quantum efficiency (QE), often necessitated relatively short exposure times, particularly on bright sources or in regions of high sky background. The shortest exposure time available for a full 1024 × 1024 detector readout was 0.2 seconds. However, faster readout times could be achieved using sub-arrays − 0.08 seconds for a 512 × 512 sub-frame and 0.015 sec for a 64 × 64 pixel sub-frame. An additional "movie mode" was available to sample a single 512 × 512 quadrant at ~0.08 seconds without any deadtime between images, or down to the 32 × 32 sub-frame (closest to the detector center) at < 0.015 seconds.

2.3 OBSERVING MODES

FLITECAM had two main observing configurations: imaging and spectroscopy. A chart showing all of the available modes and observing configurations of FLITECAM is given in Figure 3. These modes/configurations are described below in more detail.

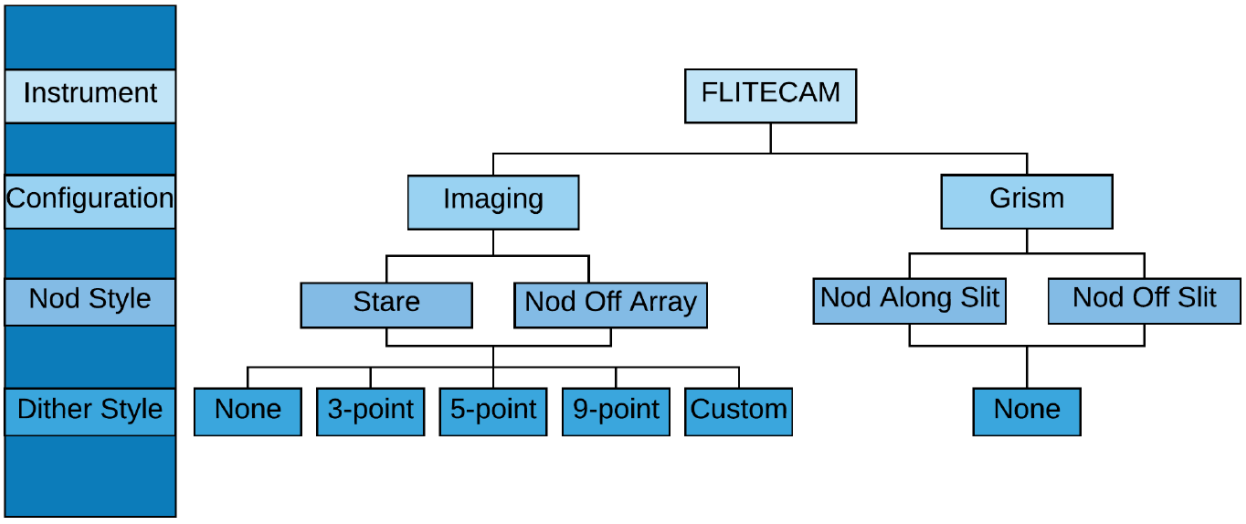

Figure 3 *A chart showing all available observing modes and observing configurations that were available with FLITECAM.*

For imaging, the filter names, adopted effective wavelengths (λ_{eff}) in micrometers, and bandwidths ($\Delta\lambda$) in micrometers are given in Table 3. Their transmission profiles are shown in Figure 4. The filter mean and pivot wavelengths, which are different for the FLITECAM-only and FLIPO configurations, are given in Appendix C. The transmission profile data can be downloaded from the FLITECAM webpage at IRSA.

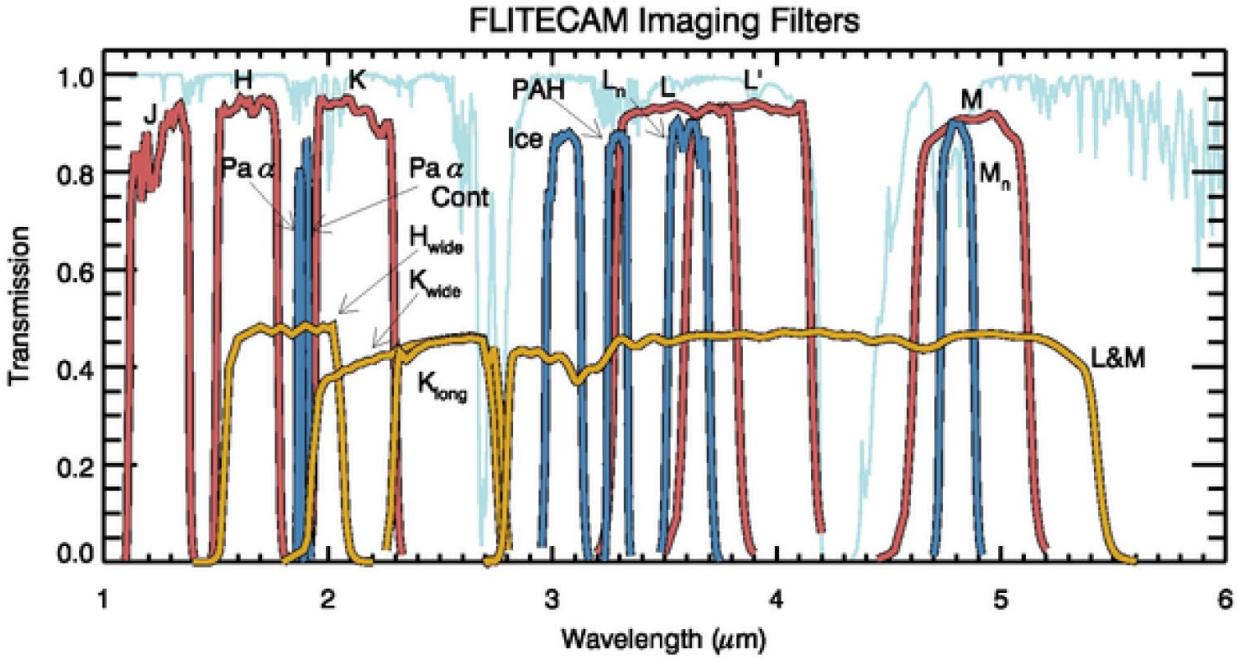

Figure 4 *FLITECAM filter transmission curves overlayed on an ATRAN model of the atmospheric transmission (light blue) assuming a zenith angle of 45° and 7 μm of precipitable water vapor. The transmission profiles of the broadband filters are shown in red, narrow and specialty filters are shown in blue, and order sorting filters (OSFs) in gold. The OSF transmission profiles have been scaled by 50% for clarity.*

For spectroscopy, the grism names, wavelength coverages in micrometers, and spectral resolutions for the wide and narrow slits are given in Table 2.

Before discussing the different observing modes of FLITECAM, it is necessary to describe the general observing techniques employed in the near-infrared. Generally, the main issue with observing in the near-infrared is that the background due to sky emission can be relatively high (compared to optical imaging) and must be removed in order to achieve high signal on the source of interest. However, background levels are not as high with FLITECAM on SOFIA, and so the chopping secondary mirror is not used, as is the case with the other longer wavelength instruments on SOFIA. Therefore, as with most ground-based near-infrared instruments, the telescope is moved throughout an observation in order to sample and ultimately subtract off sky/background emission. In any given pixel on a detector, the total number of counts is given by the sum of the counts from the dark current, telescope emission, sky background, and the target itself. Since the sky level can vary significantly over short timescales in the near infrared, it is typical to take pairs of observations back-to-back and subtract them in order to remove the dark current, telescope signal, and sky signal (to first order). An A frame exposure of the target is immediately followed

by a telescope movement and then a B frame exposure containing only sky at the target's position in the A frame:

$$A = dark + telescope + skyA + target$$
$$B = dark + telescope + skyB$$
$$A - B = target + (skyA - skyB)$$

Note that it is assumed that the sky level may vary somewhat between frame A and frame B, but the dark current and telescope emission do not. This residual sky emission can be very low or completely removed if the time between the A and B frames is less than the variation timescale of the sky background. However, further residuals can also be removed in post-processing.

For FLITECAM imaging, there were two observing modes: stare and nod-off-array.

Stare Mode: In stare mode, an observation was made without moving the telescope (or the secondary), in a manner similar to the kinds of observations made in the optical. This mode was typically used for observing point sources or compact sources that did not occupy a large region on the array. In this case, the telescope was usually moved a small amount (known as dithering) between successive images. The flat field and sky frames were then generated from the dithered observations themselves. The dither movements must be larger than the typical size of the object(s) being observed, otherwise the sky frame would contain excess emission from the location where the source overlapped in the two images.

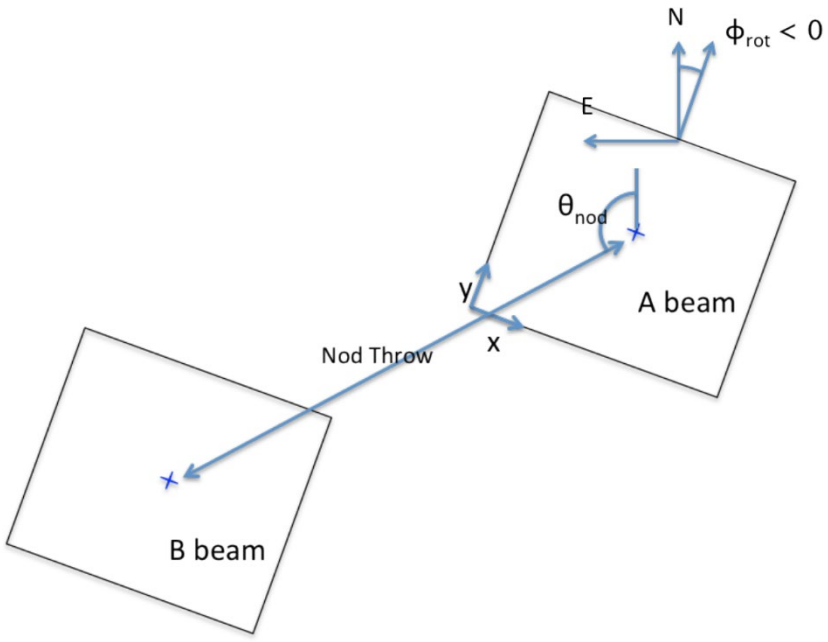

Figure 5 *Schematic of the nod-off-array mode used for imaging extended sources. The "nod throw" determines how far off the array the telescope nods, and θ_{nod} determines the angle of the nod throw, which is defined in either instrument coordinates (i.e., x,y) or sky coordinates (i.e., degrees east of north).*

Nod-Off-Array Mode: In this mode (Figure 5), which was often used for extended objects or for regions with large numbers of point sources distributed across the field, an image was taken of the source field (nod position A) and then the telescope was moved (nodded) off the source to a region without any sources ('sky' region at nod position B). Then the telescope was moved back to the source, a small adjustment to the position was applied (a dither) and the sequence was begun again. The typical observing sequence was A−B−B−A, but A−B−A−B was also frequently used. Interleaving the source and sky frames in this manner was a way of tracking the variations in the sky levels and thereby improving the quality of the sky subtraction and flat fielding. The frames acquired in the sky position were then combined to generate the sky background frame and the flat field frame. These were subtracted from and divided into (respectively) the individual source frames. After sky subtraction and flat fielding, the source frames could be aligned and combined. If the integration times were short, it could be more efficient instead to obtain a set of dithered images of the source region (A−A−A−…) and then move the telescope off the source to the sky position and take another set of dithered images (B−B−B…). The nod-off-array mode is similar to the C2NC2 mode used for FORCAST observations with the obvious exception that chopping was not used for FLITECAM observations.

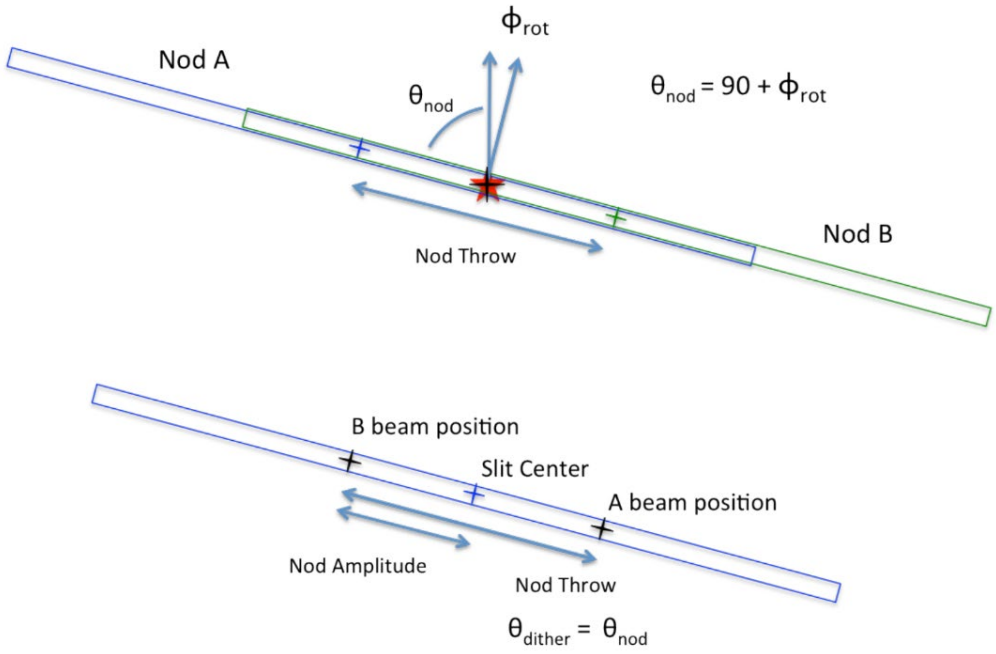

Figure 6 *Schematic of the nod-along-the-slit mode for spectroscopic observations of compact sources.*

Both of these modes could be used with or without dithers. Most FLITECAM observations were performed either in stare mode with dithers (for uncrowded fields of view) or nod-off-array with dithers (for crowded and extended emission fields of view).

FLITECAM grism observations offered two modes for producing A-B pairs: nod-along-slit and nod-off-slit.

Nod-Along-Slit Mode: The A frame was taken with the target positioned one-third to one-quarter of the distance along the slit. After the A frame was complete, the telescope moved to place the target approximately the same distance from the other end of the slit (Figure 6). The exposure taken in this configuration was the B frame. It was typical, then, to repeat A-B pairs in either an A-B-A-B or A-B-B-A sequence until the total desired integration time was achieved. In this mode, the A frame provided the sky measurement at the target position for the B frame, and the B frame provided the sky for the A frame. This mode was useful as long as the target was compact, relative to the slit length.

Nod-Off-Slit Mode: The A frame was taken with the target at the center of the slit. The B frame was taken with the target completely off the slit, so that the exposure contained only the sky signal (Figure 7). In this mode, the B frame existed only to provide the sky measurement at the target position for the A frame, which could be useful if the target was significantly extended. In this mode, too, either the A-B-A-B or A-B-B-A observing sequence could be used.

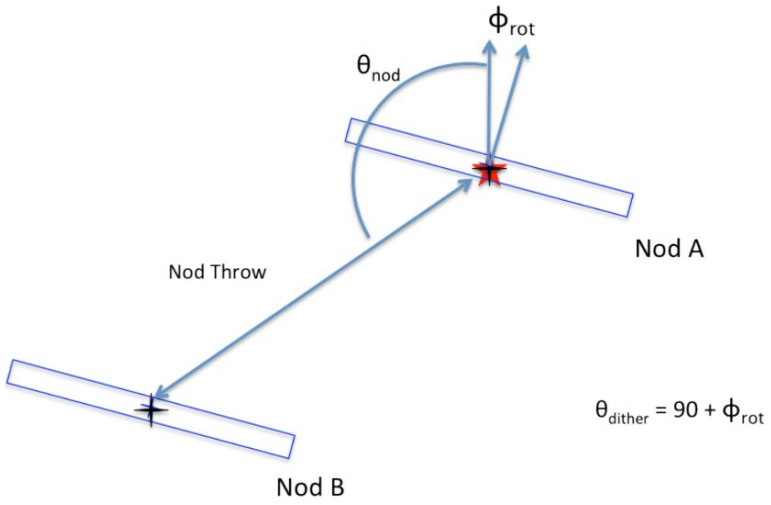

Figure 7 *Schematic of the nod-off-slit mode for spectroscopic observations for extended sources.*

3. INSTRUMENT PERFORMANCE

As the bulk of the FLITECAM instrument commissioning was performed in the co-mounted FLITECAM/HIPO (FLIPO) mode, some of the FLITECAM-only observation modes lack detailed performance characteristics. The lack of circulation of stratospheric air down the Naysmyth tube which kept the FLIPO fore-optics at cabin temperature was believed to greatly increase the observed background and may have had some effect on image quality.

Because FLITECAM was never accurately characterized at wavelengths beyond ~3 μm, the L and M band filters were offered on a shared risk basis.

3.1 BEAM / IMAGE QUALITY

Unlike some of the SOFIA instruments working at longer wavelengths, FLITECAM image quality was a product of several factors, many of which changed from flight to flight, within a flight, or as a function of target-specific issues. Therefore, unlike other long-wavelength SOFIA instruments, FLITECAM image quality was highly variable.

Issues affecting image quality of FLITECAM data are:

Telescope jitter

Jitter is the name given to the vibrations of the telescope produced by the movement of the aircraft as well as environmental winds and gusts. The opening in the cavity of the plane housing the telescope was not covered by a window but was open to the outside environment. Though the aircraft fuselage was designed to minimize turbulent airflow over the cavity opening (i.e., shear layer turbulence), it was not perfect, and winds could directly drive oscillations in the top end of the telescope. Reflections of the winds within the telescope cavity (i.e., cavity turbulence) could also jostle the telescope. Additionally, at the high altitudes the aircraft flew, it could encounter high-speed jet streams and gusts, and the angle of incidence of the aircraft with such winds could also affect the amount of jitter.

Aircraft altitude

Tests have shown that the higher the aircraft altitude, the less wind-driven telescope vibrations were observed (i.e., jitter) and the better the image quality of the observations were.

Telescope elevation

Test have also shown that there was a general trend in image quality due to the elevation (i.e., the angle from the horizon) of the telescope during the observations, with the worst image quality generally being encountered at telescope elevations near 45° and the best at the upper (~58°) and lower (~23°) elevation limits of the telescope. This effect however was very subtle.

Aircraft turbulence

The active optics of the SOFIA telescope could maintain the telescope pointing under light turbulence, however there could be some degradation of image quality during turbulent episodes.

Active optics precision

As described above for aircraft turbulence, SOFIA had an active control system that corrected telescope pointing multiple times a second. This could reduce the effects of telescope jitter and turbulence. However, these systems were fine-tuned over the course of the first three SOFIA observing cycles, and thus image quality in general improved over that time as well. Therefore,

early-cycle FLITECAM data in general has poorer image quality than later cycles (i.e., Cycles 4-6).

Table 2 gives the average image quality observed during FLITECAM commissioning for most filters, however the L and M band filters were never fully characterized and were never used for science. Furthermore, these data were taken in the FLIPO mode (i.e., with FLITECAM co-mounted with HIPO) and there may be differences (besides those mentioned above) in the image quality encountered between those data and data taken with FLITECAM mounted to the telescope by itself.

3.1.1 PSF Stability Over Time

The FLITECAM image size showed no evidence of systematic variation during its years of operation. The angular resolution measured in each filter is shown in Table 2, together with a standard deviation of the measurements. Any long-term trend is smaller than this scatter which is likely dominated by seeing and focus variations among the limited number of calibration observations.

3.2 POINTING PERFORMANCE / ASTROMETRIC ACCURACY

Every observation began with the source acquisition, where the telescope was pointed to the planned coordinates specified in the Astronomical Observation Request (AOR) of the observation. The header keywords "OBSRA" and "OBSDEC" record this position. The pointing accuracy of the telescope in acquiring objects was expected to be accurate to 1″ (Temi et al. 2018).

For imaging mode data, the astrometry of the data can be corrected to better than the 1″ pointing accuracy, if needed. Since the field of view of the FLITECAM data is very large, comparisons of typical fields with Spitzer or 2MASS data should provide multiple point sources for which to adjust the FLITECAM astrometry.

In spectroscopic mode, after initial acquisition, the telescope positioning was tweaked if needed to ensure the source was placed, centered, in the proper place on the slit. However, though never formally quantified or studied, it is known observationally from data from SOFIA's mid-infrared instrument FORCAST that the telescope pointing could drift over a flight by ~1-2″, possibly due to the telescope/optics temperature changes over the course of each flight.

3.3 SENSITIVITY

Users of FLITECAM archive data can calculate detection limits directly from the data, however below the estimated sensitivities of FLITECAM data in both imaging and spectroscopic modes will be presented.

3.3.1 Imaging Sensitivities

Imaging sensitivities are shown in Figure 8. The as-measured imaging sensitivities in the FLIPO (combined FLITECAM+HIPO) mode are shown in yellow. Since the sensitivity values for the FLITECAM-only mode were never fully characterized, the theoretical sensitivity values are shown in red in this figure.

Atmospheric transmission affects sensitivity, particularly at wavelengths >4 μm, depending on the water vapor overburden. FLITECAM was never accurately characterized at these longer

wavelengths in either the FLIPO or FLITECAM-only mode, and though the L and M band filters were offered on a shared risk basis, they were never actually used for science.

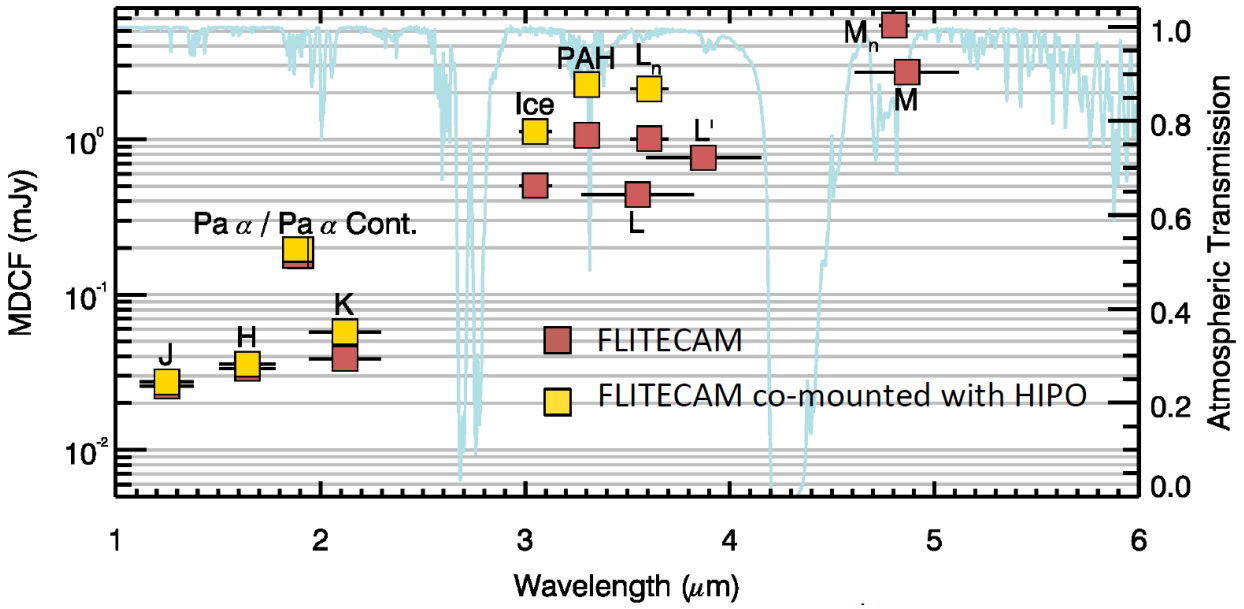

Figure 8 *FLITECAM imaging sensitivities for both FLITECAM-only (red) and FLIPO (i.e. co-mounted with HIPO; yellow) modes for all FLITECAM imaging filters (see Table 2). The left axis is the minimum detectable continuum flux (MDCF) in Jy to achieve a S/N of 4 in 900 s with a PWV overburden of 7 μm. Horizontal bars correspond to the photometric band pass of each filter. The blue line is the atmospheric transmission (right axis) from ATRAN models.*

3.3.2 Grisms Sensitivities

Spectroscopic sensitivities are shown in Figure 9. Since the sensitivity values for the both FLIPO and FLITECAM-only modes were never fully characterized, the theoretical sensitivity values are shown in blue and green, respectively, in this figure.

As with imaging sensitivities, atmospheric transmission significantly affects spectroscopic sensitivity, at wavelengths >4 μm, worsening with higher water vapor overburden conditions.

3.3.3 Sensitivities of FLITECAM-Only vs. FLIPO Configurations

The relative sensitivity between the FLITECAM and FLIPO (FLITECAM + HIPO co-mounted) configurations was assessed by comparing the calibration factors derived for standard stars on flights in each configuration through seven different filters. Calibration factor is in units of DN/sec/Jy, where DN is the "data number" (number of photoelectrons times gain) in an image. A higher value of the calibration factor means more signal on the detector. The average of the ratios between FLITECAM and FLIPO are 1.11 ± 0.04, indicating 11% of the light is lost in the FLIPO configuration due to the extra dichroic in the optical path. There is no wavelength dependence of this ratio. The actual sensitivity in the FLITECAM-only configuration is therefore approximately 11% better than in FLIPO configuration.

3.3.4 Saturation

The FLITECAM detector well depth was relatively shallow (~ 80,000 e) which, when combined with the detector quantum efficiency (QE), often necessitated relatively short exposure times, particularly on bright sources or in regions of high sky background.

When FLITECAM was co-mounted with HIPO, the background emission was much higher in the thermal infrared (i.e., $\lambda \geq 3$ μm). Imaging observations past 3 μm could not be achieved in full-frame mode, and required using smaller subarrays which could be read out fast enough to avoid saturation. Similarly, spectroscopic observations past 4 μm were not possible at all in the FLIPO configuration. However, when FLITECAM was mounted by itself to the telescope, full-frame imaging observations were possible out to 4 μm, and the full suite of FLITECAM grisms could be used without issue.

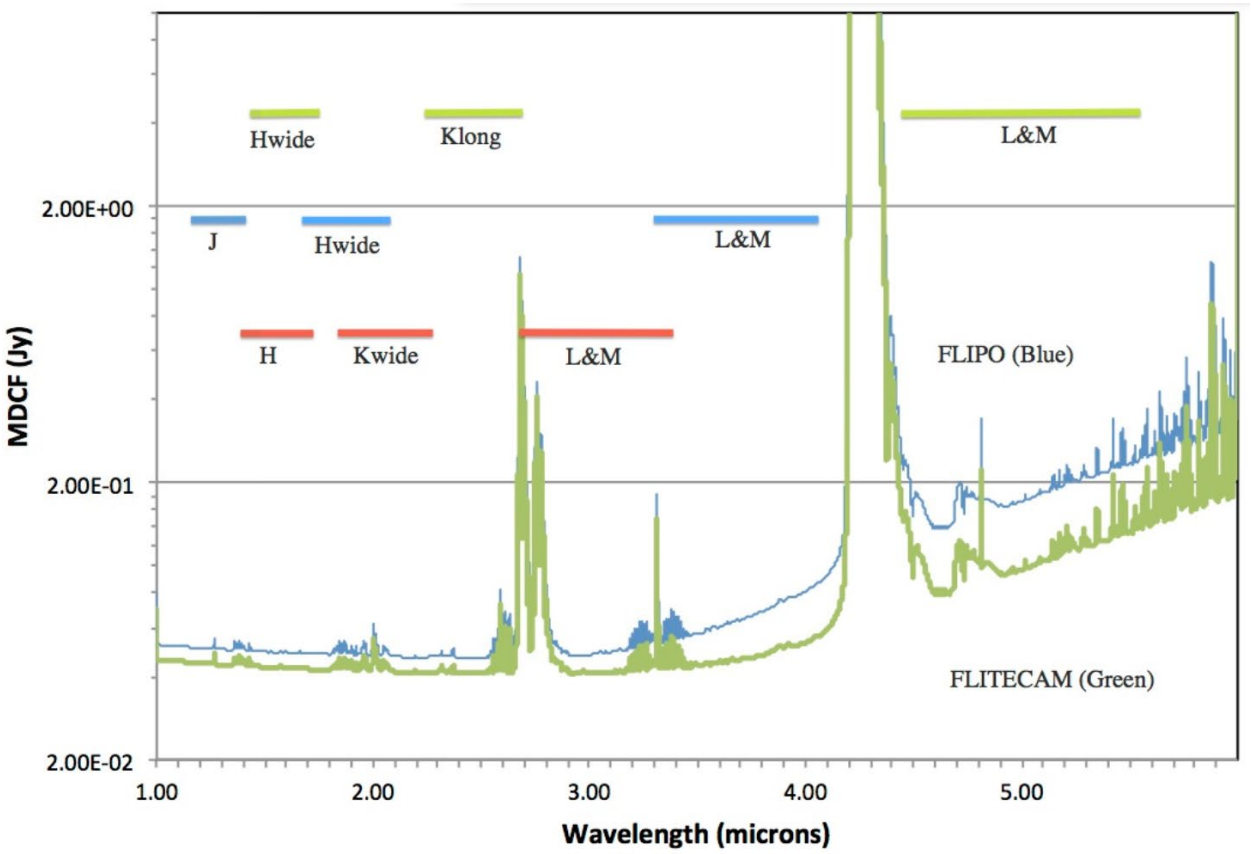

Figure 9 *Theoretical continuum point source sensitivities for the FLITECAM grisms combined with an ATRAN model of the atmospheric transmission. The Minimum Detectable Continuum Flux (MDCF; 80% enclosed energy) in Jy is shown for a S/N of 4 in 900 s at a water vapor overburden of 7.3 μm, an altitude of 41K feet, and an elevation angle of 45° (i.e., at an airmass of 1.4) for FLITECAM-only (green) and FLIPO (blue). Horizontal bars show the grism bandpasses. Green bars are for the three orders of Grism A, blue bars are for the three orders of Grism B, and red bars are for the three orders of Grism C (see Table 3).*

Care had to be taken not to over-expose the detector since charge persistence can be a significant problem for InSb arrays. If the detector was over-exposed, it was necessary to take several long exposures (~5 minutes each) of blanks mounted in the filter wheel to allow the detector to recover.

3.4 FLUX CALIBRATORS AND FLUX CALIBRATION ACCURACY

3.4.1 Flux Calibration Accuracy

There are two types of flux calibration error: relative and absolute. Relative flux error refers to how repeatable (precise) the measurements are from observation to observation. The final uncertainties in calibrated FLITECAM images and spectra contain only the estimated statistical uncertainties due to the noise in the image or the extracted spectrum (i.e., relative error). The systematic uncertainties due to this calibration process are recorded in header keywords. For imaging data, the error on the calibration factor is recorded in the keyword ERRCALF. For grism data, the estimated overall fractional error on the flux is recorded in the keyword CALERR.

Earlier versions of this pipeline (i.e., prior to REDUX version 2.0.0) may have stored the systematic calibration error in the error spectrum or variance image, added in quadrature with the statistical error. Check PIPEVERS and compare the error estimates for the calibrated products to earlier products to ensure correct interpretation of the error estimates.

Absolute flux error refers to how accurate observations are at producing measured flux values consistent with a known flux quantity.

3.4.1.1 Imaging Relative Flux Error

The RMS error in the ERRCALF values in the FITS headers (derived across multiple calibrators and flights) are typically on the order of about 6%. Again, this error is mostly the statistical measurement error.

3.4.1.2 Imaging Absolute Flux Error

Because most of the calibration stars are mildly varying and stellar models are also not perfect (see, for example, Dehaes et al. 2011), there is an additional uncertainty that must be applied to derived FLITECAM imaging fluxes, which is on the order of 3-6%. Combined, the above relative error and this error give the "absolute" flux calibration error.

3.4.1.3 Grism Relative Flux Error

Comparisons between the calibrated FLITECAM spectra of standard stars and their models show deviations on the order of about 5-10% rms. This error value is recorded in the keyword CALERR in the grism data headers.

3.4.1.4 Grism Absolute Flux Error

Experience using A0V stars to calibrate near-infrared data shows the overall error in the absolute flux calibration to be about 10-20% (for more see Section 4.4.2). However, because slit losses could be variable during a science observation (due to varying image quality and, perhaps, slit drift) as well as for calibration observations, absolute flux calibration of FLITECAM spectra required additional photometric observations taken in FLITECAM imaging mode. Spectra could then be scaled to match the photometric points to achieve absolute flux calibration. Because this

final calibration step is dependent upon the imaging photometry absolute flux error, the error described must be combined with the grism relative error to obtain the spectroscopic absolute flux error.

3.4.2 Flux Calibrator Variability Over Time

The stability of FLITECAM was assessed by comparing the calibration factors (which are the ratio of the "true" to measured calibrator flux) between flight series in 2014 February, 2015 October, 2016 October, and 2017 October. The instrument was in the FLIPO configuration for the first and last of these flight series, and it was in the FLITECAM for the middle two flight series. There is no evidence for a monotonic trend of instrument response over time. The difference in calibration factors between the 2015, 2016, and 2017 flight series, relative to 2014, was -3.5%, +5%, and -9%. The differences may be due to the window transmission or other factors in the instrument; however, there is significant scatter of 10% in the calibration factors, partly due to the limited number of calibration observations performed.

3.4.3 FLITECAM Flux Calibrators

Photometric standards for FLITECAM were chosen from three sources: (1) bright stars with spectral classifications of A0V as listed in SIMBAD; (2) Landolt SA stars (K giants and A0-4 main sequence stars) listed as 'supertemplate' stars in Cohen et al. (2003); and (3) K giant stars listed as 'spectral template' stars in Cohen et al. (1999). For all of these objects, models were either available (from the Cohen papers) or derivable (from a model of Vega for the A0V stars). Use of the A0V stars required scaling the Vega model to the observed magnitudes of the target and reddening the model to match the observed color excess of the target. It should be noted that A0V stars had to be used to calibrate the Paschen α filter, as these objects have a strong absorption feature in this band. The models of the spectral template K giants listed in Cohen et al. (1999) extend down only to 1.2 μm, and therefore could not be used to calibrate the J band filter.

For spectroscopic data, calibrator targets were also typically A0V stars with stellar models constructed from a model of Vega.

Since FLITECAM used only a limited set of stellar and asteroid calibrators to flux calibrate imaging and spectroscopy data, all such calibrators are given in Table 4. The table also includes Plan IDs for each calibrator for ease of finding them in the IRSA archive. (All SOFIA calibrators had Plan IDs prefixed with 90).

For more on calibration procedures, see Section 4.4. For a list of imaging flux calibration factors and their errors for all filters, see Appendix B.

Table 4: FLITECAM Calibrators with Plan ID Numbers

Plan ID	Target
90_0017	HD 71155
90_0017	HIP 30762
90_0069	Gamma Aqr
90_0070	SAO 34401

Plan ID	Target
90_0081	HD 216735
90_0081	HR 3163
90_0081	HD 66664
90_0087	SA 92-336

Plan ID	Target
90_0076	HD 26579
90_0076	HD 370
90_0076	HD 58142
90_0077	HD 5319
90_0079	76 Dra
90_0079	HD 41695

Plan ID	Target
90_0087	HIP 92396
90_0088	SA 113-269
90_0088	SA 115-516
90_0088	SA 113-269
90_0088	SA 115-516
90_0088	HD 203856

3.5 FIELD ORIENTATION / GRISM SLIT ROTATION ACCURACY

Since the instrument mounting flange on the SOFIA telescope had over 20 fixed mounting bolts, the orientation of the FLITECAM instrument was for all practical purposes the same each time it was installed on the telescope. However, the optical system as a whole (which included FLITECAM) may have suffered from flexure or slight misalignments that may have caused minor distortion in the field that can be seen as a rotation from one observation to another. Furthermore, improper definition of the telescope boresight (i.e., optical axis) while observing (or as defined in the reduction software) may also have caused small errors in the rotation. This rotation error was never calculated specifically for FLITECAM, however using FORCAST as a proxy, the rotation error measured was typically very close to zero (<0.5°), though the largest single variations ever measured have been +1.1° and -0.5°. Thus, a maximum deviation of the rotation of approximately ± 1° is estimated for field orientation in imaging mode and slit orientation in grism mode.

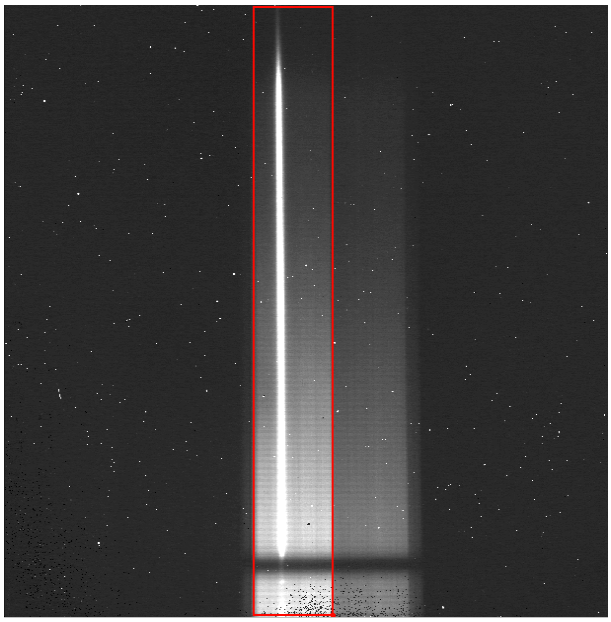

Figure 10 *A typical raw FLITECAM grism observation taken with the wide slit. As with the raw imaging data, there are hot pixels scattered across the frame. The wide-slit region is outlined in red; the narrow-slit region is visible to the right of the wide-slit region. Wavelength increases from the bottom to the top of the frame*

Since the SOFIA telescope was not an equatorially mounted telescope, the field of view during an observation rotated over time. Unlike many non-equatorial mounted telescopes, SOFIA did not have a field de-rotator either (and one was not built into FLITECAM), and so this meant the angle of the slit on sky for spectroscopy could not be set at a desired angle, and therefore the slit orientation depended on where and when the object was observed. Thus, for any given Level 2 data product (i.e., a single FLITECAM observation) the error in the known orientation of the slit on a source is the same as that of the field rotation given above (i.e., ± 1°). However, as a spectroscopic target was observed, the slit rotated on the source with a speed dependent on the sky rotation rate. This means that the final co-add of all Level 2 data into a final Level 3 spectrum may include data from many different slit orientations. This can particularly cause problems interpreting data where the source was extended.

3.6 GRISM WAVELENGTH CALIBRATION AND ACCURACY

For spectroscopic data, spatial and spectral distortions are corrected for by defining calibration images that assign a wavelength coordinate (in μm) and a spatial coordinate (in arcsec) to each detector pixel within the slit region of the detector (see Figure 10). Each 2D spectral image in an observation is clipped and resampled into a rectified spatial-spectral grid, using these coordinates to define the output grid. If appropriate calibration data is available, the output from this step is an image in which wavelength values are constant along the columns, and spatial values are constant along the rows, correcting for any curvature in the spectral trace (Figure 11).

Since no calibration lamps were installed in FLITECAM, wavelength calibration was generated from identifications of sky emission and telluric absorption lines and a polynomial fit to centroids of those features in pixel space for each row (i.e., along the dispersion direction). The default wavelength calibration of archival FLITECAM data is expected to be good to within approximately one pixel in the output spectrum.

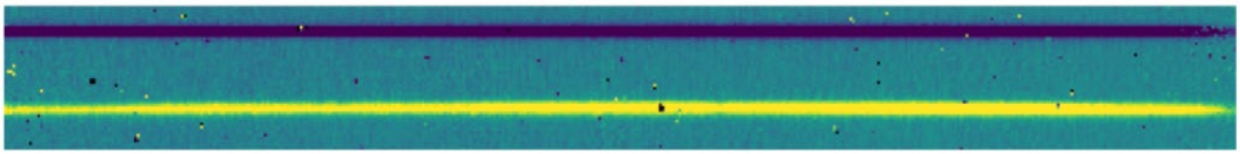

Figure 11 *A nod-along-slit spectral image after pair-subtraction and after rectification, with wavelength in x and spatial extent in y. Black pixels are bad pixels which will be properly handled later in the spectral extraction process.*

For some observational cycles, sufficient calibration data may not be available, resulting in some residual spectral curvature, or minor wavelength calibration inaccuracies in the archival data. See the Section 4.1.2.4 for more.

3.7 USABLE FIELD

The detector in FLITECAM was large enough to cover most of the approximately 8.0 arcminute field of view delivered by the SOFIA telescope. However, due to the combination of FLITECAM having an internal circular field stop (to minimize scattered light) and the presence of severe coma at the edges of the full 8′ field, data from FLITECAM are cropped to a 5.6′ × 5.6′ size (see Figure 12).

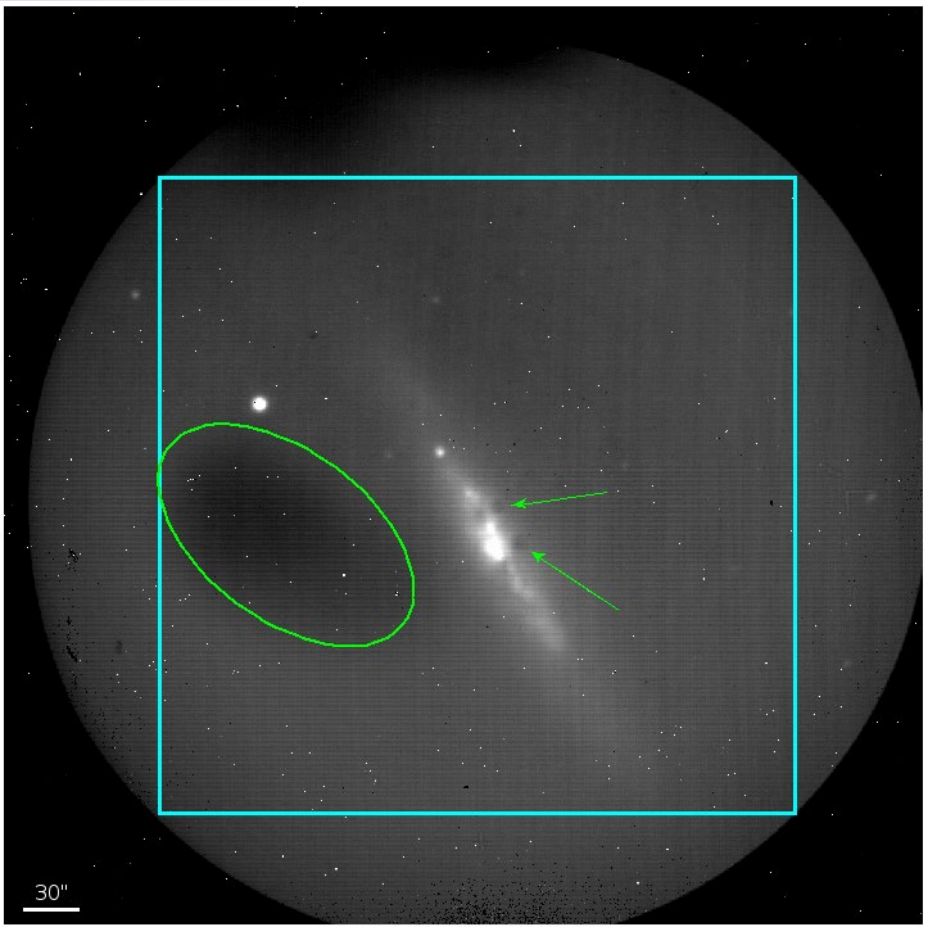

Figure 12 *A typical FLITECAM image obtained during a commissioning flight. A circular field stop restricts the field projected onto the square array. The cyan box represents the usable portion of the remaining field. Sources that fall outside of this box show too much coma for accurate PSF measurement. The small white dots visible in the image are hot pixels. The green ellipse encompasses a region of low quantum efficiency, and the green arrows show obscurations in the optical path.*

3.8 BAD PIXELS

The detector in FLITECAM was fairly clean, cosmetically speaking. Though there were several dead pixels and "hot" pixels (Figure 12), they were spaced out with no large dead areas (or dead columns/rows) or bad pixel groupings that would be more problematic to deal with. Bad pixel masks are made as part of the data reduction process and are saved as the third extension of the FLITECAM FITS files.

3.9 ARRAY FLATNESS AND FLAT FIELDING

Flat-field frames are needed to permit correction for fixed-pattern noise in the array and large-scale distortions caused by various telescope and/or instrument optical issues. Imaging flats for FLITECAM are made from images of the sky. In nod-off-array mode, dithered sky images are used to generate a flat that is used to correct all on-source images. In stare mode, the dithered source images themselves are used to generate the flat. For each source image, a different flat is created from the remaining source images in order not to introduce correlations in the gain correction. There are two gross features seen in the raw FLITECAM data that are corrected along

with other minor gain variations via the flat fielding process: 1) The elliptical area of lower quantum efficiency that is intrinsic to the detector itself (see Figure 12); and 2) several dark "spots" on the field that are likely due to obscurations in the telescope and/or instrument optical path (see Figure 12).

An example of FLITECAM data showing these features and being corrected by the flat-fielding process of the SOFIA pipeline is given in Figure 13.

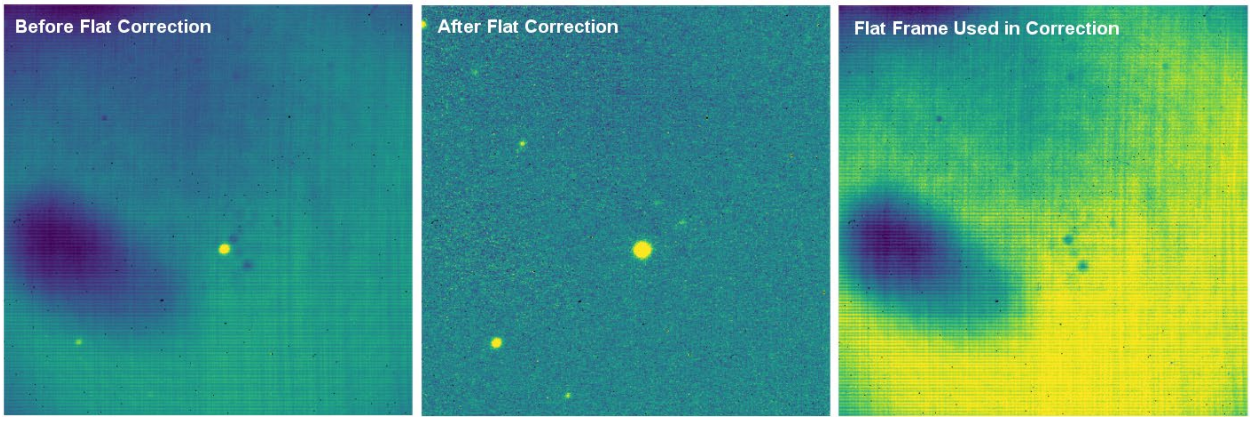

Figure 13 *(Left) A clipped stare mode image from one dither position of an observation and before flat field correction; (Middle) The same field corrected for gain variations after the application of a flat frame;(Right) The normalized flat frame used to correct the data, derived from the remaining dithers in the observation.*

4. DATA

FLITECAM data and format are described below. More information about the data format as well as specifics of the pipeline processing of the data can be found in the FLITECAM Pipeline User's Manual, available at the SOFIA website at IRSA: FLITECAM Pipeline User's Manual.

4.1 PIPELINE UPDATES

The FLITECAM REDUX data reduction pipeline software and the data products it creates have gone through several updates over time. In particular, the recent update to version 2.0.0 introduced some relatively large changes to the format of the data that may require updates to any local routines used to analyze the data.

Below is a table summarizing major changes by pipeline version. Dates refer to approximate release dates. Check the PIPEVERS key in FITS headers to confirm the version used to process the data, as some early data may have been reprocessed with later pipeline versions.

More detailed change notes are available in *Appendix D: Change notes for the FLITECAM pipeline* in FLITECAM Pipeline User's Manual (FLITECAM Pipeline User's Manual).

Table 5: Examples of Important FLITECAM REDUX Pipeline Change Notes

Version	Date	Software/Cycle	Comments
1.0.0	01/23/15	IDL:Cycle 1,2	Integrated FLITECAM imaging algorithms (FDRP) with Spextool spectral extraction algorithms, in the standard pipeline interface (Redux)
1.0.1	05/14/15	IDL:Cycle 3	Flux calibration incorporated into pipeline, rather than applied as a separate step. EXPTIME keyword updated to track total nominal on-source integration time.
1.1.0	09/20/16	IDL:Cycle 4/5	Flux calibration factors are now applied to data arrays to convert them to physical units (Jy). The calibrated data product has file code CAL (PRODTYPE=calibrated). COA files are no longer designated Level 3, even if their headers contain calibration factors. Grism calibration incorporated into the pipeline, using stored instrumental response files, similar to the FORCAST grism calibration process.
1.2.0	12/15/17	IDL:Cycle 4/5	Overall improvement to calibration. Updated to include TEL files which are similar to REG files with telluric corrections applied to each file. Final calibrated file CAL file is same as COA file but with calibration factor (CALFCTR) already applied. Improved telluric correction for FLITECAM grism data.
2.0.0	08/16/21	Python	File format of FITS files for imaging updated from image cube to separate extensions. Extensions are now

			FLUX, ERROR, and EXPOSURE. ERROR now represents the standard deviation (sigma) rather than the variance (σ^2). Grism data formats also changed significantly. Grism images and spectra are stored in the same FITS file, under separate extensions. Final 1D spectra (CMB files, PRODTYPE=combined_spectrum) are still stored in the same format as before; the spectrum corresponds to the SPECTRAL_FLUX extension in the COA (PRODTYPE=coadded_spectrum) file.

4.2 DATA QUALITY

Data quality for FLITECAM is recorded in the FITS keyword DATAQUAL and can contain the following values:

NOMINAL: No outstanding issues with processing, calibration, or observing conditions.
USABLE: Minor issue(s) with processing, calibration, or conditions, but should still be scientifically valid (perhaps with larger than usual uncertainties); see HISTORY records for details.
PROBLEM: Significant issue(s) encountered with processing, calibration, or observing conditions; may not be scientifically useful (depending on the application); see HISTORY records for details. In general, these cases are addressed through manual reprocessing before archiving and distribution.
FAIL: Data could not be processed successfully for some reason. These cases are rare and generally not archived or distributed to the GI but mentioned in emails and updates regarding program progress.

Any issues found in the data or during flight are recorded as QA Comments and emailed to the GI after processing and archiving. A permanent record of these comments is also directly recorded in the FITS files themselves. Check the FITS headers, near the bottom of the HISTORY section, under such titles as “Notes from quality analysis” or “QA COMMENTS”.

4.3 DATA PRODUCTS AND NAMING CONVENTIONS

4.3.1 File Naming Conventions

FLITECAM output files from Redux are named according to the convention:

FILENAME = F[flight]_FC_IMA|GRI_AOR-ID_SPECTEL1_Code_FN1[-FN2].fits

where flight is the SOFIA flight number, *FC* is the instrument identifier, *IMA* or *GRI* specifies that it is an imaging or grism file, AOR-ID is the eight digit AOR identifier for the observation, *SPECTEL1* is the keywords specifying the filter or grism used, *Code* is three letters identifying the product type (listed in Table 6 and Table 7 below), and *FN1* is the file number corresponding to the input file. *FN1-FN2* is used if there are multiple input files for a single output file, where *FN1* is the file number of the first input file and *FN2* is the file number of the last input file.

4.3.2 Pipeline Products

The following tables (Table 6 and Table 7) list all intermediate products generated by the present version (v2.0.0) of the pipeline for imaging and grism modes, in the order in which they are produced. By way of showing these intermediary data products, these tables also indicate the steps taken in the data reduction process (left column) and how the data were corrected by the pipeline to produce the final data products. Note that earlier versions of this pipeline produced different sets of default products; one must refer to earlier revisions of the FLITECAM Pipeline User's Manual if the PIPEVERS key in FITS headers indicate an early pipeline version was used.

The product type is stored in the FITS headers under the keyword PRODTYPE. By default, for imaging, the *flat*, *telluric_corrected*, *coadded*, and *calibrated* products are saved. For spectroscopy, the *spectral_image*, *rectified_image*, *spectra*, *spectra_1d*, *calibrated_spectrum*, *coadded_spectrum*, and *combined_spectrum* products are saved.

The final grism mode output product from the Combine Spectra or Combine Response steps are dependent on the input data: for OBSTYPE=STANDARD_TELLURIC, the *instrument_response* is produced instead of a *coadded_spectrum* and *combined_spectrum*.

For most observation modes, the pipeline additionally produces an image in PNG format, intended to provide a quicklook preview of the data contained in the final product.

Table 6: Intermediate FLITECAM Data Products for Imaging Reductions

Step	Data type	PRODTYPE	PROCSTAT	Code	Saved	Extensions
Correct Nonlinearity	2D image	linearized	LEVEL_2	LNZ	N	FLUX, ERROR, BADMASK
Clip Image	2D image	clipped	LEVEL_2	CLP	N	FLUX, ERROR, BADMASK, EXPOSURE
Make Flat	2D image	flat	LEVEL_2	FLT	Y	FLUX, ERROR, BADMASK, EXPOSURE, FLAT, FLAT_ERROR, FLAT_BADMASK
Correct Gain	2D image	gain_ corrected	LEVEL_2	GCR	N	FLUX, ERROR, BADMASK, EXPOSURE
Subtract Sky	2D image	background_ subtracted	LEVEL_2	BGS	N	FLUX, ERROR, BADMASK, EXPOSURE
Register	2D image	registered	LEVEL_2	REG	N	FLUX, ERROR, BADMASK, EXPOSURE

Step	Data type	PRODTYPE	PROCSTAT	Code	Saved	Extensions
Telluric Correct	2D image	telluric_ corrected	LEVEL_2	TEL	Y	FLUX, ERROR, BADMASK, EXPOSURE
Coadd	2D image	coadded	LEVEL_2	COA	Y	FLUX, ERROR, EXPOSURE
Flux Calibrate	2D image	calibrated	LEVEL_3	CAL	Y	FLUX, ERROR, EXPOSURE
Mosaic	2D image	mosaic	LEVEL_4	MOS	Y	FLUX, ERROR, EXPOSURE

Table 7: Intermediate FLITECAM Data Products for Spectroscopy Reduction

Step	Data type	PRODTYPE	PROCSTAT	Code	Saved	Extensions
Correct Nonlinearity	2D spectral image	linearized	LEVEL_2	LNZ	N	FLUX, ERROR, BADMASK
Make Spectral Image	2D spectral image	spectral_ image	LEVEL_2	IMG	Y	FLUX, ERROR
Stack Dithers	2D spectral image	dithers_ stacked	LEVEL_2	SKD	N	FLUX, ERROR
Make Profiles	2D spectral image	rectified_ image	LEVEL_2	RIM	Y	FLUX, ERROR, BADMASK, WAVEPOS, SLITPOS, SPATIAL_MAP, SPATIAL_PROFILE
Locate Apertures	2D spectral image	apertures_ located	LEVEL_2	LOC	N	FLUX, ERROR, BADMASK, WAVEPOS, SLITPOS, SPATIAL_MAP, SPATIAL_PROFILE
Trace Continuum	2D spectral image	continuum_ traced	LEVEL_2	TRC	N	FLUX, ERROR, BADMASK, WAVEPOS, SLITPOS, SPATIAL_MAP, SPATIAL_PROFILE, APERTURE_TRACE
Set Apertures	2D spectral image	apertures_set	LEVEL_2	APS	N	FLUX, ERROR, BADMASK, WAVEPOS, SLITPOS, SPATIAL_MAP,

Step	Data type	PRODTYPE	PROCSTAT	Code	Saved	Extensions
						SPATIAL_PROFILE, APERTURE_TRACE, APERTURE_MASK
Subtract Background	2D spectral image	background_ subtracted	LEVEL_2	BGS	N	FLUX, ERROR, BADMASK, WAVEPOS, SLITPOS, SPATIAL_MAP, SPATIAL_PROFILE, APERTURE_TRACE, APERTURE_MASK
Extract Spectra	2D spectral image; 1D spectrum	spectra	LEVEL_2	SPM	Y	FLUX, ERROR, BADMASK, WAVEPOS, SLITPOS, SPATIAL_MAP, SPATIAL_PROFILE, APERTURE_TRACE, APERTURE_MASK, SPECTRAL_FLUX, SPECTRAL_ERROR, TRANSMISSION
Extract Spectra	1D spectrum	spectra_1d	LEVEL_3	SPC	Y	FLUX
Calibrate Flux	2D spectral image; 1D spectrum	calibrated_ spectrum	LEVEL_3	CRM	Y	FLUX, ERROR, BADMASK, WAVEPOS, SLITPOS, SPATIAL_MAP, SPATIAL_PROFILE, APERTURE_TRACE, APERTURE_MASK, SPECTRAL_FLUX, SPECTRAL_ERROR TRANSMISSION, RESPONSE, RESPONSE_ERROR
Combine Spectra	2D spectral image; 1D spectrum	coadded_ spectrum	LEVEL_3	COA	Y	FLUX, ERROR, EXPOSURE, WAVEPOS, SPECTRAL_FLUX, SPECTRAL_ERROR TRANSMISSION, RESPONSE
Combine Spectra	1D spectrum	combined_ spectrum	LEVEL_3	CMB	Y	FLUX
Make Response	1D response spectrum	response_ spectrum	LEVEL_3	RSP	Y	FLUX

Step	Data type	PRODTYPE	PROCSTAT	Code	Saved	Extensions
Combine Response	1D response spectrum	instrument_ response	LEVEL_4	IRS	Y	FLUX

4.4 FLUX CALIBRATION PROCEDURE

This section describes the process for deriving imaging and spectral calibrations. For more information on flux calibration accuracy and the selection of flux calibrators, see Section 3.4.

4.4.1 Imaging

The reduction process, up through image coaddition, generates Level 2 images with data values in units of counts per second (ct/s or DN/s). After Level 2 imaging products are generated, the pipeline derives the flux calibration factors (in units of ct/s/Jy or DN/s/Jy) and applies them to each image. The calibration factors are derived for each FLITECAM filter configuration from observations of calibrator stars.

After the calibration factors have been derived, the coadded flux is divided by the appropriate factor to produce the Level 3 calibrated data file, with flux in units of Jy/pixel. The value used is stored in the FITS keyword CALFCTR.

The calibration is carried out in several steps. The first step consists of measuring the photometry of all the standard stars for a specific mission or flight series, after the images have been corrected for the atmospheric transmission relative to that for a reference altitude and zenith angle. The atmospheric transmission in each filter has been computed using the ATRAN code (Lord 1992) for a range of observatory altitudes (corresponding to a range of overhead precipitable water vapor values) and telescope elevations. The ratio of the transmission at each altitude and zenith angle relative to that at the reference altitude (41,000 feet) and zenith angle (45°) has been calculated for each filter and fit with a low order polynomial. The ratio appropriate for the altitude and zenith angle of each observation is calculated and applied to each image.

The pipeline performs aperture photometry on the reduced Level 2 images of the standard stars after the registration stage using a photometric aperture radius of 12 pixels (about 5.7″ for FLITECAM). The telluric-corrected photometry of the standard star is related to the measured photometry of the star via

$$N_e^{std,corr} = N_e^{std} \frac{R_\lambda^{ref}}{R_\lambda^{std}}$$

where the ratio $R_\lambda^{ref} / R_\lambda^{std}$ accounts for differences in system response (atmospheric transmission) between the actual observations and those for the reference altitude of 41,000 feet and a telescope elevation of 45°. Similarly, for the science target, we have

$$N_e^{obj,corr} = N_e^{obj} \frac{R_\lambda^{ref}}{R_\lambda^{obj}}$$

Calibration factors (in ct/s/Jy or DN/s/Jy) for each filter are then derived from the measured photometry (in ct/s or DN/s) and the known fluxes of the standards (in Jy) in each filter. These predicted fluxes were computed by multiplying a model stellar spectrum by the overall filter + instrument + telescope + atmosphere (at the reference altitude and zenith angle) response curve and integrating over the filter passband to compute the mean flux in the band. The adopted filter throughput curves (available at the IRSA FLITECAM website) are those provided by the vendor. The instrument throughput is calculated by multiplying an estimate of the instrumental optics transmission (0.80) and the detector quantum efficiency (0.56). The FLITECAM overall throughput is (0.285). The telescope throughput value is assumed to be constant (0.85) across the entire FLITECAM wavelength range.

The calibration factor, *C*, is computed from

$$C = \frac{N_e^{std,corr}}{F_\nu^{nom,std}\left(\lambda_{ref}\right)} = \frac{N_e^{std,corr}}{\langle F_\nu^{std}\rangle}\,\frac{\lambda_{piv}^2}{\langle\lambda\rangle\lambda_{ref}}$$

with an uncertainty given by

$$\left(\frac{\sigma_C}{C}\right)^2 = \left(\frac{\sigma_{N_e^{std}}}{N_e^{std}}\right)^2 + \left(\frac{N_{\langle F_\nu^{std}\rangle}}{\langle F_\nu^{std}\rangle}\right)^2$$

Here, λ_{piv} is the pivot wavelength of the filter, and $\langle\lambda\rangle$ is the mean wavelength of the filter (see Appendix C, Table 12). The calibration factor refers to a nominal flat spectrum source at the reference wavelength λ_{ref}.

The calibration factors derived from each standard for each filter are then averaged. The pipeline inserts this value and its associated uncertainty into the headers of the Level 2 data files for the flux standards and uses the value to produce calibrated flux standards. The final step involves examining the calibration values and ensuring that the values are consistent. Outlier values may come from bad observations of a standard star; these values are removed to produce a robust average of the calibration factor across the flight series. The resulting average values are then used to calibrate the observations of the science targets.

Using the telluric-corrected photometry of the standard, $N_e^{std,corr}$ (in ct/s), and the predicted mean fluxes of the standards in each filter, $\langle F_\nu^{std}\rangle$ (in Jy), the flux of a target object is given by

$$F_\nu^{norm,obj}\left(\lambda_{ref}\right) = \frac{N_e^{obj,corr}}{C}$$

where $N_e^{obj,corr}$ is the telluric-corrected count rate in ct/s detected from the source, C is the calibration factor (ct/s/Jy), and $F_\nu^{norm,obj}\left(\lambda_{ref}\right)$ is the flux in Jy of a nominal, flat spectrum source (for which $F_\nu \sim \nu^{-1}$) at a reference wavelength λ_{ref}.

The values of $C, \sigma_c,$ and λ_{ref} are written into the headers of the calibrated (PROCSTAT = LEVEL_3) data as the keywords CALFCTR, ERRCALF, and LAMREF, respectively. The reference wavelength λ_{ref} for these observations was taken to be the mean wavelengths of the filters, $\langle\lambda\rangle$.

Note that σ_c, as stored in the ERRCALF value, is derived from the standard deviation of the calibration factors across multiple flights. These values are typically on the order of about 6%. There is an additional systematic uncertainty on the stellar models, which is on the order of 3-6%.

For a list of imaging flux calibration factors (CALFCTR) and their errors (ERRCALF) for all filters, see Appendix B.

4.4.1.1 Color Correction

An observer often wishes to determine the true flux of an object at the reference wavelength, $F_\nu^{obj}(\lambda_{ref})$, rather than the flux of an equivalent nominal, flat spectrum source. To do this, a color correction K is defined such that

$$K = \frac{F_\nu^{norm,obj}(\lambda_{ref})}{F_\nu^{obj}(\lambda_{ref})}$$

where $F_\nu^{norm,obj}(\lambda_{ref})$ is the flux density obtained by measurement on a data product. Divide the measured values by K to obtain the "true" flux density. In terms of the wavelengths defined above,

$$K = \frac{\langle\lambda\rangle\,\lambda_{ref}}{\lambda_{piv}^2}\,\frac{\langle F_\nu^{obj}\rangle}{F_\nu^{obj}(\lambda_{ref})}$$

For most filters and spectral shapes, the color corrections are small (<10%).

4.4.2 Spectroscopic Grism

The common approach to characterizing atmospheric transmission for ground-based infrared spectroscopy is to obtain, for every science target, similar observations of a spectroscopic standard source with as close a match as possible in both airmass and time. Such an approach is not practical for airborne observations, as it imposes too heavy a burden on flight planning and significantly lowers the overall science efficiency of a flight. Therefore, a calibration plan is employed that incorporates a few observations of a calibration star per flight and a model of the atmospheric absorption for the approximate altitude and airmass (and precipitable water vapor, if known) at which the science objects were observed.

Instrumental response curves are generated from the extracted spectra of calibrator targets, typically A0V stars with stellar models constructed from a model of Vega. The extracted spectra are corrected for telluric absorption using the ATRAN models corresponding to the altitude and zenith angle of the calibrator observations, smoothed to the nominal resolution for the grism/slit combination, and sampled at the observed spectral binning. The telluric-corrected spectra are then divided by the appropriate models to generate response curves (with units of ct/s/Jy at each wavelength) for each grism passband. The response curves derived from the various calibrators for each instrumental combination are then combined and smoothed to generate a set of master instrumental response curves. The statistical uncertainties on these response curves are on the order of 5-10%.

Flux calibration of FLITECAM grism data for a science target is currently carried out in a two-step process:

1. For any given observation of a science target, the closest telluric model (in terms of altitude and airmass of the target observations) is selected and then smoothed to the observed resolution and sampled at the observed spectral binning. The observed spectrum is then divided by the smoothed and re-sampled telluric model.

2. The telluric-corrected spectrum is then divided by a response function corresponding to the observed instrument mode to convert DN/s to Jy at each pixel.

In order to account for any wavelength shifts between the models and the observations, an optimal shift is estimated by minimizing the residuals of the corrected spectrum, with respect to small relative wavelength shifts between the observed data and the telluric spectrum. This wavelength shift is applied to the data before dividing by the telluric model and response function.

Based on our experience with FORCAST calibration, and with using A0V stars to calibrate near-infrared data, the overall error in the flux calibration is expected to be about 10-20%. However, the uncertainty on the slope of the calibrated spectrum should be substantially less than that, on the order of a few percent (see e.g., Rayner et al. 2009). The Level 3 data product for any grism includes the calibrated spectrum and an error spectrum that incorporates these RMS values. The adopted telluric absorption model and the instrumental response functions are also provided in the output product.

As for any slit spectrograph, highly accurate absolute flux levels from FLITECAM grism observations (for absolute spectrophotometry, for example) require additional photometric observations to correct the calibrated spectra for slit losses that can be variable (due to varying image quality) between the spectroscopic observations of the science target and the calibration standard.

4.1 KNOWN ISSUES / ARTIFACTS & MITIGATION

FLITECAM data is known to have some issues that affect the data quality or leave residual artifacts (after correction by the pipeline) to varying degrees. This section covers some of these issues, notes their severity, occurrence, and if the issue is fixable.

Relatedly, the quality assessment (QA) comments that can be found in the HISTORY of the FITS headers of the FLITECAM data should always be checked for exact information on any data issues.

4.1.1 Imaging Issues/Artifacts

4.1.1.1 Optical Distortion of Field

Occurrence: All data.

Significance: The large field of view of FLITECAM is subject to field distortions due to imperfections of the instrument optics. Though a mask is used to exclude areas of the FLITECAM images with very high coma, there is still clearly optical distortion of the field when comparing FLITECAM imaging data to, say, 2MASS imaging data. This optical distortion was not fully characterized, and this distortion is not corrected by the pipeline software. It is estimated that, nominally, the uncertainty in the WCS solution is 0.7″ near the reference pixel (i.e., that given by CRPIX1 and CRPIX2 in the headers) and that this increases to ~3″ near the frame edge.

Fix: None, using the pipeline software, but if there are sufficient sources on the field to compare to imaging data from another facility in theory a transformation matrix could be created to correct the data.

4.1.1.2 Inaccurate WCS

Occurrence: Occasionally.

Significance: As stated in the previous section, it is estimated that the nominal uncertainty in the WCS solution is 0.7″ near the reference pixel (i.e., that given by CRPIX1 and CRPIX2 in the headers) and that this increases to ~3″ near the frame edge. However, there are occasionally much larger inaccuracies (up to ~10″) in the WCS due to problems encountered when acquiring the source or field.

Fix: Comparisons to imaging data from other facilities like 2MASS or Spitzer can be used to correct the WCS. The faulty WCS information may also be corrected by rerunning the pipeline and using centroiding or cross-correlation between images to identify common sources in the registration step. In this case, the first image is taken as the reference image, and calculated offsets are applied to the WCS header keywords (CRPIX1 and CRPIX2) in all subsequent images. Earlier versions of the pipeline reduced data in the archive had applied registration to the images themselves, rather than to the WCS in the FITS header, interpolating them into the same spatial grid. As of v2.0.0, registration affects only the CRPIX1 and CRPIX2 keywords in the header.

4.1.1.3 Debris on Detector

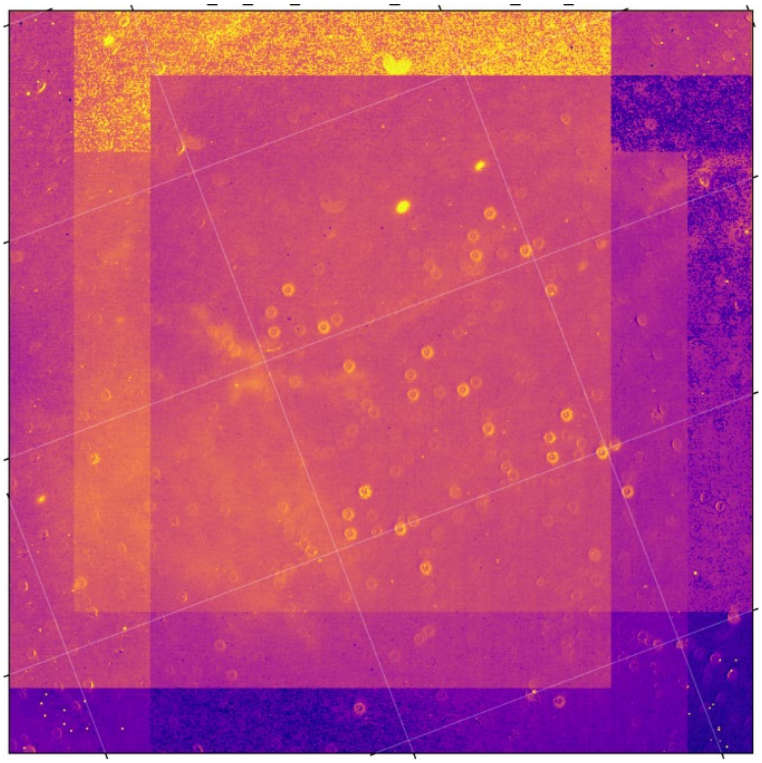

Figure 14 *An image taken on Flight 337 through the PAH329 filter. Dappled across the field are droplet-looking features due to the presences of debris/liquid on the FLITECAM entrance window.*

Occurrence: OC4J flight series

Significance: At some point prior to the first flight of the OC4J flight series for FLITECAM, some debris and/or liquid had gotten onto the entrance window of the instrument. It was discovered during observations on the first flight of that series and persisted throughout the entire flight series

(the entrance window is not easily accessible). The main issue created by this debris/liquid is that it produced artifacts across the field of the imaging observations (Figure 14). Sometimes sky frame correction helped, and sometimes it made the issue worse.

Fix: None.

4.1.2 Spectroscopy Issues/Artifacts

4.1.2.1 Grism C Light Leak

Occurrence: All data taken with Grism C.

Significance: While reviewing the FLITECAM spectral performance during commissioning, a consistent increase in the background at the short wavelength end of the C grism spectra was noted in all the spectroscopic setups (i.e., FLT_C2_LM, FLT_C3_Kw, and FLT_C4_H). This increase in background was not present in the A or B grism data with the same blocking filters. This "grism C light leak" is shown in Figure 15. In addition, a bright background region was seen at the top of the FLITECAM array in imaging mode when the long wavelength filters (λ>2.2μm) were tested during commissioning, but these filters were never used for science. It is expected that this effect is ratioed out when dividing by the standard star spectrum, but the issue was never fully characterized. Therefore, the short wavelength end of the C grism spectra may be unreliable.

Fix: None.

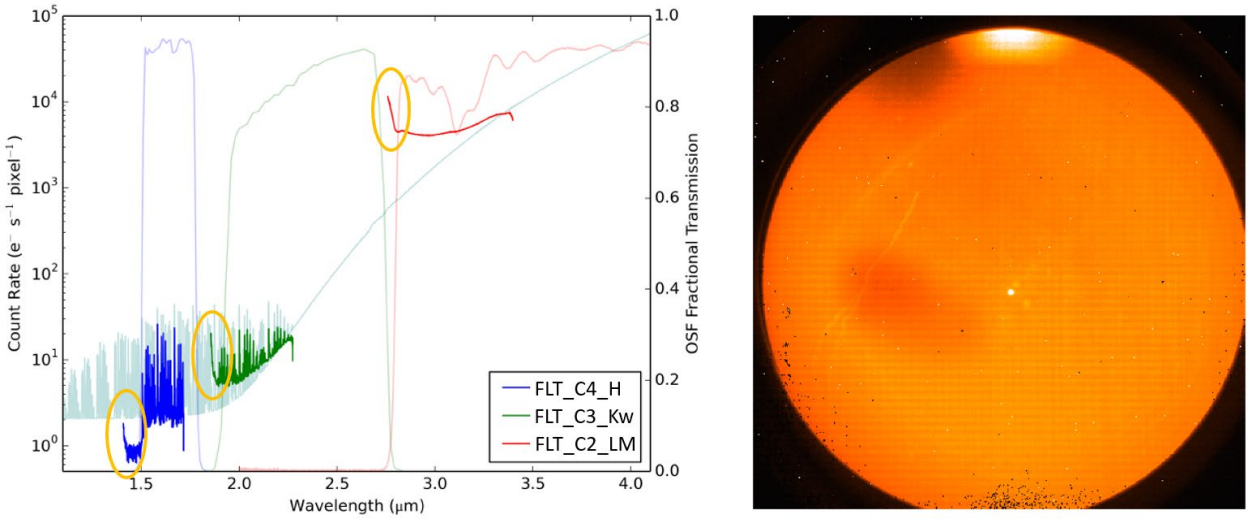

Figure 15 *(Left) Bold red, green, and blue lines are actual spectra taken in each of the C grism setups (FLT_C2_LM, FLT_C3_Kw, and FLT_C4_H, respectively). Shown in light red, green, and blue are the blocking filter transmission curves for those same setups, while pale grey is a theoretical spectral model. Circled in orange are the areas of the observed spectra that are affected by the light leak. (Right) A L-band image showing a bright feature at the top of the array due to the light leak.*

4.1.2.2 Inaccurate WCS

Occurrence: Occasionally.

Significance: This is a minor issue since care was made to ensure that the requested target for observation was the proper source in the slit during grism observations. However, occasionally the WCS may not accurately reflect the true position of the source.

Fix: No fix necessarily needed, though the WCS CRPIX1 and CRPIX2 values could be updated.

4.1.2.3 No Grism Flat Fielding

Occurrence: Occasionally.

Significance: A suitable flat field was not derived for some data. In addition, sometimes the spectra cross a region of low QE that is difficult to correct for in the flat fielding procedure at longer wavelengths. Consequently, sometimes it was determined not to combine the "A" and "B" beam spectra for observations that were nodded along the slit (refer to Section 3.2 for a description of the use of A and B beams). In these cases, the data for each beam were stored as separate apertures in the final, combined spectrum file.

Fix: None.

4.1.2.4 Lack of Sufficient Calibration Data

Occurrence: Rarely (and all 1″ grism observations in the OC2A flight series).

Significance: Sometimes there are insufficient calibration data to fully process the science data. In particular, in the OC2A flight series the grism observations using the 1″ slit could not be processed due to lack of sufficient calibration data. Another example in calibration maps is the rectification of the 2D grism spectra, which are generated from identifications of sky emission and telluric absorption lines. For some grism observations, sufficient calibration data may not be available, resulting in some residual spectral curvature, or minor wavelength calibration inaccuracies.

Fix: Usually none. However, for the rectification case, the spectral curvature can be compensated for in sources with strong continuum emission by tracing the continuum center during spectral extraction (see the FLITECAM Pipeline Users Manual). For other sources, a wider aperture may be set, at the cost of decreased signal-to-noise.

4.1.2.5 CH_4 Residuals

Occurrence: Flight 244.

Significance: Atmospheric CH_4 shows absorption features at 2.4 μm that are usually removed when target spectra are divided by the standard star spectra. Due to a bad standard-object conditions mismatch on Flight 244, all K-band grism data (i.e., FLT_A2_KL data) have very strong telluric CH_4 residuals and thus flux values in the spectra for $\lambda > 2.7$ μm may be unreliable.

Fix: None.

5. SCIENTIFIC RESULTS

With SOFIA flying above 99% of the atmospheric water vapor content, the transmission of infrared light from 3-5 μm was significantly improved compared to any ground-based telescope working in the near-infrared. Designed to perform imaging in selected bands over the wavelength range 1.0-5.5 μm, FLITECAM served as an instrument that filled the gap between the wavelength region where ground-based observations are significantly hampered by the thermal background emission from both the telescope and the atmosphere and the considerably longer infrared wavelengths that constituted the primary focus of SOFIA's design. With the colder, drier air and colder telescope (~240 K), FLITECAM on SOFIA was an order of magnitude more sensitive in the 3-5 μm region than at ground-based sites.

One advantage FLITECAM had over concurrent space-borne near-infrared instruments was the ability to perform narrow band imaging in the 2-5 μm regime. Additionally, FLITECAM had an advantage over ground-based near-infrared facilities because it had access to spectral lines and features totally or partially absorbed by telluric water vapor. To take advantage of this in its imaging mode, FLITECAM was outfitted with three narrow-band filters that covered three such lines/features that were difficult or impossible to observe from the ground: the Paschen-α (Paα) line at 1.88 μm, the 3.3 μm polycyclic aromatic hydrocarbon (PAH) feature, and the 3.08 μm water-ice feature. In its spectroscopic mode, FLITECAM had grisms that were designed to cover the entire 1-5 μm spectral region at a resolution of R~1300. Not only did these grisms cover the same spectral features as the imaging filters described above, but there are also additional interesting atomic and molecular lines which fall into the FLITECAM grism bands such as Si VI at 1.96 μm and a methane (C_2H_2) band at 2.6 μm, which again were impossible or difficult to observe from ground-based facilities.

Gaining access to all these spectral lines/features at stratospheric altitudes is beneficial because they are of astronomical importance. Paα is valuable for studying star formation within highly extinguished environments due to its strong penetrating power, while prevalence of PAH emission in a wide variety of astronomical sources (e.g., star forming regions, planetary nebulae, and external galaxies) has made it a critical topic for astronomical research. Studying the presence and origins of water in the universe, as observed with the 3.08 μm water-ice feature, is a significant area of investigation due to its connection to life. Moreover, the Si VI line is a good tracer of active galactic nuclei, and methane is a useful probe in planetary and brown dwarf research.

FLITECAM was also designed to be able to quickly read-out its array multiple times a second, which combined with the mobility of SOFIA, allowed for occultation studies in the near-infrared. Occultations occur when a celestial body moves in front of a star, eclipsing the star's light. This causes a "path of totality" similar to a solar eclipse where the shadow moves across the surface of the Earth. Therefore, airborne observations are superior to those conducted on the ground, since ground-based observations are often hindered by unfavorable weather conditions, and often the path of the occultation shadow doesn't pass over land. In contrast, an airborne telescope can be positioned anywhere at any time and have its flight path optimized based on the latest predictions right up to just hours before the event.

Detailed below are a few FLITECAM science results highlighting its unique capabilities. The first result (Section 5.1) demonstrates FLITECAM's ability to map out the 3.3um PAH feature in a variety of galactic environments with its narrow band filters. The second result (Section 5.2) demonstrates FLITECAM's ability to perform spectroscopy on objects where the most important

spectral features in the near-infrared are partly or totally unobservable from ground-based telescopes. Perhaps the most unique and exciting observing scenario for FLITECAM was its ability to observe occultations. In Section 5.3, FLITECAM's observations of the 2015 occultation of Pluto are described, which enabled study of its peculiar atmosphere.

5.1 CHARACTERIZING PAH EMISSION

- Principle Investigators: *O. Berné (Université de Toulouse), E. Peeters (University of Western Ontario), and T. Tielens (Leiden Observatory)*
- Plan IDs: 02_0056, 03_0032, 04_0058

Publications:

- Tracing PAH Size in Prominent Nearby Mid-Infrared Environments, C. Knight et al. (2021a), ApJ, 918, 8
  DOI: 10.3847/1538-4357/ac02c6
- Mapping PAH Sizes in NGC 7023 with SOFIA, B. Croiset et al. 2016, A&A, 590, 26
  DOI: 10.1051/0004-6361/201527714
- Characterizing the PAH Emission in the Orion Bar, C. Knight et al. (2021b), MNRAS, 509, 3523
  DOI: 10.1093/mnras/stab3047

Polycyclic aromatic hydrocarbon (PAH) molecules are central to understanding the physical and chemical processes occurring in interstellar and circumstellar environments. Recent findings suggest that UV photons are intimately involved in the transformation of PAH molecules, giving rise to a diverse range of organic compounds, including hydrocarbons and fullerene isomers. A distinct outcome of this chemical evolution is the alteration of PAH size distributions within specific local physical conditions, particularly in response to varying levels of UV radiation. Consequently, precise infrared observations are required to accurately limit the photochemical models that understand the variations in PAH size within the interstellar medium.

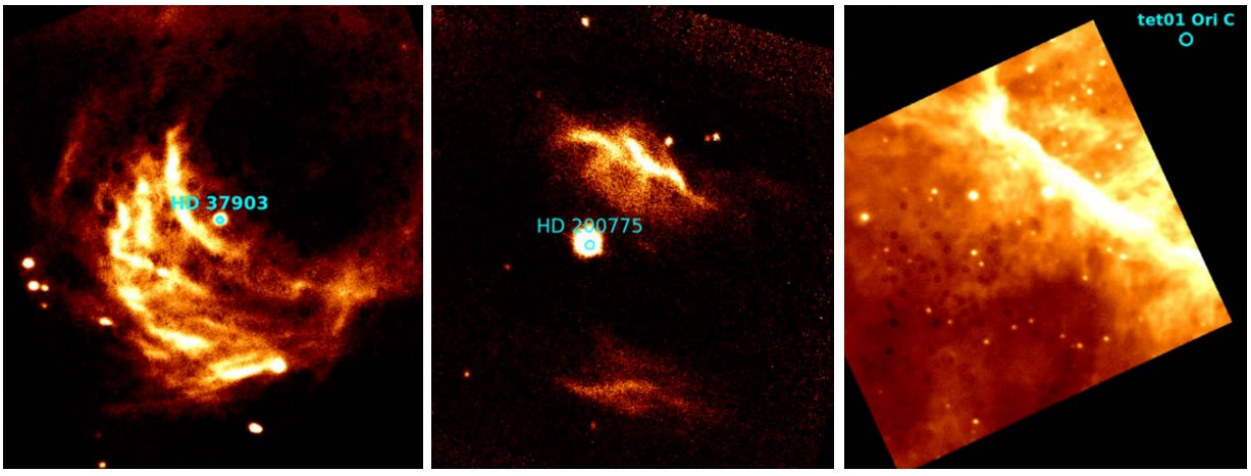

Figure 16 *FLITECAM 3.3 μm PAH filter images of (Left) reflection nebula NGC2023, (Middle)reflection nebula NGC7023, and (Right) the Orion Bar photodissociation region. The ionizing stars for each region are labeled.*

Using FLITECAM's 3.3um PAH filter, several astronomical sources/environments were imaged. Knight et al. (2021a) present such data for the reflection nebulae NGC 2023 and NGC 7023, as well as the photodissociation region of the Orion Bar (Figure 16). The 3.3 and 11.2 μm PAH band tend to be well correlated, so the FLITECAM 3.3μm data were combined with 11.2 μm data from Spitzer in the analyses. In addition to the appearance of these two spectral features varying with ionization rate, they can also be heavily influenced by changes in the chemical structure of the PAHs themselves. Both the 3.3 and 11.2 μm features originate in neutral PAHs, and their ratio is a good proxy for measuring the size of the emitting PAHs. Knight et al. (2021a) found that not only does the amount of PAH ionization decrease as one gets further from the ionizing sources in the two reflection nebulae (as one would expect), but that the average PAH size also decreases. This result seems to indicate that the UV intensity closer to the ionizing sources are causing photochemical evolution of the PAH population, destroying all but the largest PAH molecules. More surprising was the fact that no trend in PAH size vs. distance from the ionizing source could be ascertained for the Orion Bar (though PAH size did vary throughout the region). This is puzzling and may be due to the region's complex geometry.

5.2 SUPERNOVA 2014J

- Principle Investigator: *P. Garnavich (University of Notre Dame)*
- Plan ID: 02_100, 75_0001, 75_0002

Publications:

- Observations of Type Ia Supernova 2014J with FLITECAM/SOFIA, W. Vacca et al. (2015), ApJ, 804, 66
  DOI: 10.1088/0004-637X/804/1/66

Type Ia supernovae are utilized in cosmology and serve as reliable "standard candles" for measuring distances to far off galaxies, underscoring the importance of comprehending the underlying physics governing their explosions and evolution. Researchers have formulated various supernova models that can be tested against observations to scrutinize their accuracy and minimize model parameter uncertainties. In particular, near-infrared spectra of nearby and luminous Type Ia supernovae are useful in this pursuit and are particularly beneficial if they cover the entire near-infrared contiguously.

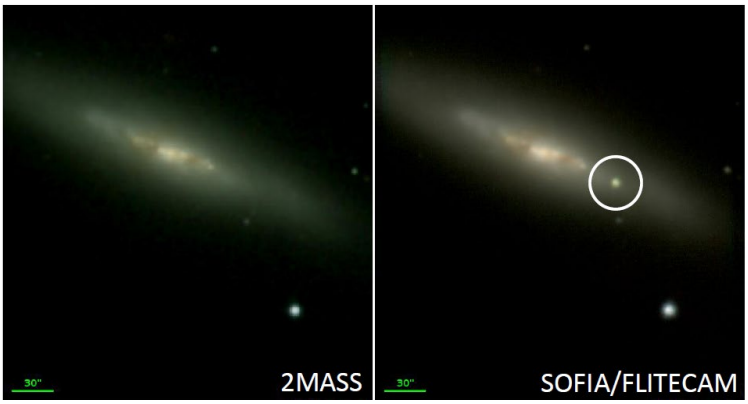

Figure 17 *(Left) 2MASS image of the M82 galaxy before and (Right) the SOFIA/FLITECAM image after the appearance of Supernova 2014J. The location of the supernova is marked by the white circle (in these images north is up and east is left).*

The occurrence of Supernova 2014J in the galaxy M82, situated relatively close at a distance of about 3.4 megaparsecs, presented an ideal opportunity to test these models. Observations were conducted using FLITECAM on multiple nights, starting roughly 35 days after the supernova event (Figure 17). Near-infrared spectra were obtained during three separate flights, each covering some portion of the total 1.1-3.4 μm observed wavelength range, and revealed notable changes over time (Vacca et al. 2015). These spectra prominently featured a sequence of spectral characteristics originating from permitted Co II and forbidden [Co III] transitions (see Figure 18).

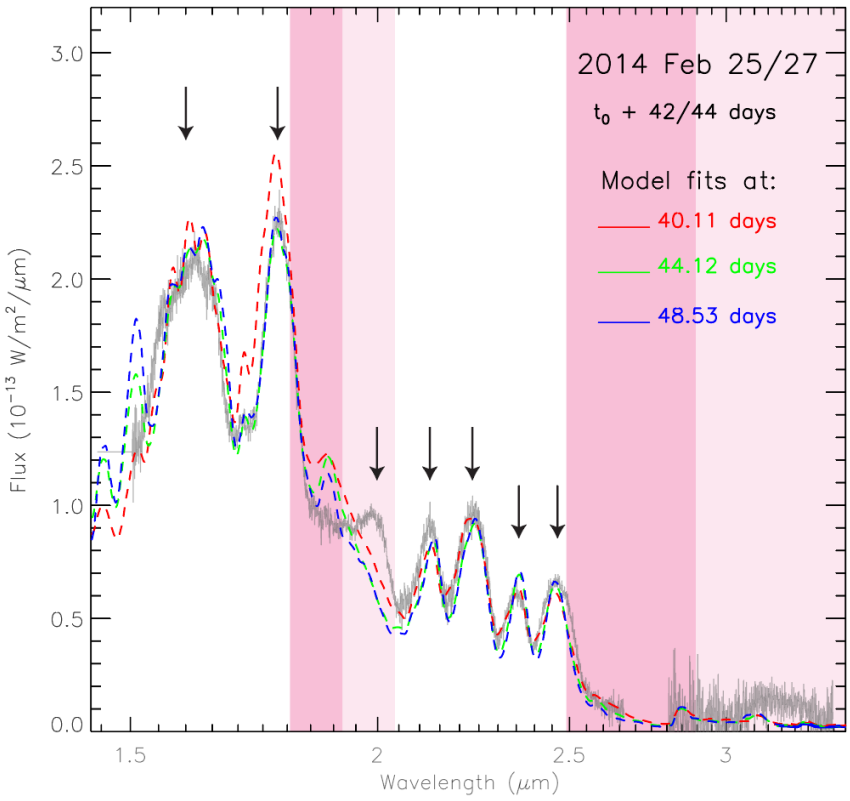

Figure 18 *FLITECAM spectra of SN2014J, with data shown in grey. The data from 1.4-2.6 μm is from Feb 25 (42 days after explosion) and data from 2.8-3.4 μm is from Feb 27 (44 days after explosion). Model fits for three different times past explosion are given by the dashed red, green, and blue lines. Downward arrows delineate the locations in the spectra where Co II and [Co III] line features are predicted to have peaks. The dark pink shading shows wavelength space where ground-based observations are impossible (atmospheric transmission <20%), and lighter pink is where ground-based observations are difficult (transmission <80%).*

The advantageous atmospheric transparency achievable in the stratosphere on board SOFIA allowed FLITECAM to capture the only dataset encompassing the complete near-infared ionized Co feature profile of SN 2014J. Notably, the 1.77 μm emission feature (attributed to a combination of Co II lines) extended into a wavelength region that is challenging to observe from terrestrial observatories. Moreover, the FLITECAM spectrum within the 3.0-3.4 μm range is believed to be the first-ever obtained for a Type Ia supernova in this specific wavelength range.

A comparison between the FLITECAM spectra and model predictions revealed generally good agreement for many features, including the 1.77 μm feature (obvious in Figure 18). However, it

was apparent that the fits were less satisfactory around the 2 μm mark and within the under-observed 3.0-3.4 μm wavelength range. While this consistency between models and observed spectra indicates a grasp of the fundamental aspects of Type Ia supernova physics and their evolution, the noted discrepancies underscore the need for further refinement and understanding of these models.

5.3 OCCULTATION OF PLUTO

- Principle Investigator: *M. Person (Massachusetts Institute of Technology)*
- Plan ID: 03_0028

Publications:

- Haze in Pluto's Atmosphere: Results from SOFIA and Ground-based Observations of the 2015 June 29 Occultation, M. Person et al. (2021), Icarus, 356, 113572
  DOI: 10.1016/j.icarus.2019.113572

Pluto has a thin atmosphere containing nitrogen (N_2), carbon monoxide (CO), methane (CH_4), and other trace gases. Close to its icy surface, this atmosphere is in a state of vapor-pressure equilibrium with the surface ices. Above the surface, the presence of methane in the atmosphere serves as a natural thermostat, helping to maintain the temperature at around 100 K. Pluto's atmospheric structure is of particular interest because the decrease in solar energy input as Pluto moves along its eccentric orbit toward aphelion is expected to lead to a reduction in atmospheric pressure or even a complete collapse of the atmosphere itself. Although some earlier models predicted that a collapse would have already begun, even the most recent observations have revealed that this is not yet the case.

On 29 June 2015, Pluto was occulted by a fairly bright star (R_{mag}~11.9). Researchers use stellar occultations such as this one as a method to gauge the temperature and pressure of a planet's atmosphere from Earth. During a stellar occultation event, the star's brightness diminishes due to refraction by the planetary atmosphere. The rate of this dimming depends on the temperature and the average molecular weight of the atmosphere. By making an assumption of a predominantly nitrogen-based atmosphere, one can then determine how the temperature varies with altitude.

The path of totality of this occultation occurred over the South Pacific, with the shadow's centerline only barely crossing land in southern New Zealand. From its airborne platform, SOFIA was able to maneuver to a more favorable position than any ground-based observatory to observe this event. FLITECAM was in its FLIPO configuration (i.e., co-mounted with the HIPO optical instrument) for these observations, which meant that the team could gather three wavelengths from the optical to near-infrared simultaneously (four wavelengths, if one counts the Focal Plane Imager camera, which is nominally used for guiding, but was used also for science in this case). This observational configuration allowed researchers to investigate the wavelength dependence of the occultation light curves.

The resultant light curves are shown in Figure 19. The flux of the star can be seen to drop on the left side of this plot before it bottoms out at about 145 seconds into the occultation. If Pluto no longer had an atmosphere this drop would be immediate, however the gradual drop indicates the atmosphere was still there, causing the star to dim more and more as it gradually moved behind more and more of the atmosphere. The bright peak in the center of the curve is due to the refraction from the atmosphere focusing of the occulting star's light like a magnifying glass – a phenomenon

that can only be seen if one is observing very close to the center of the shadow. It can be seen in Figure 19 that the flux never reaches zero. The small differences in residual flux at the light curve minimum as a function of wavelength were used to determine that there exists small-particulate haze in Pluto's atmosphere with particle sizes of ~0.1 μm in radius.

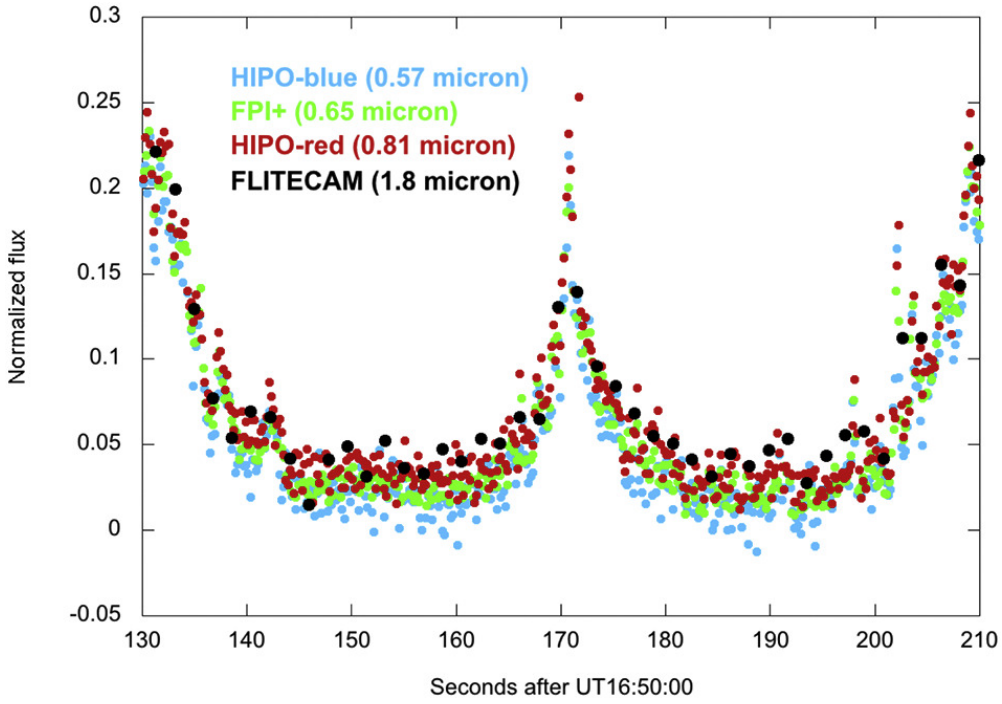

Figure 19 *Light curve of the Pluto occultation at multiple wavelengths, each taken contemporaneously from SOFIA. The minimum flux at the bottom of the light curves reaches different levels for the different wavelengths that were observed, allowing for characterization of the haze particles in Pluto's atmosphere.*

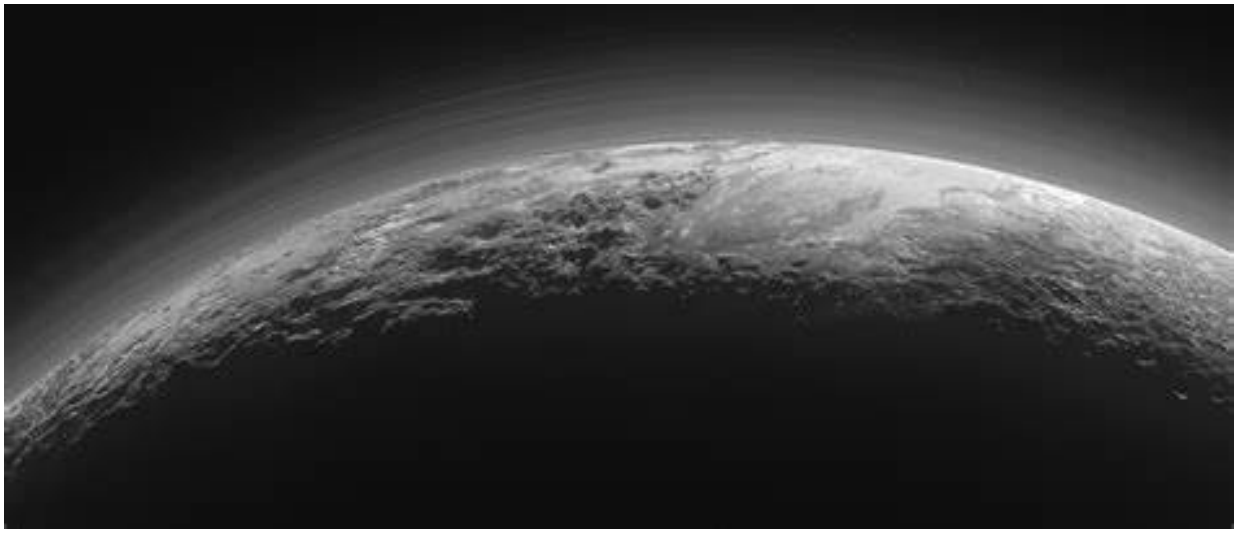

Figure 20 *An image taken from the New Horizons mission of the haze in Pluto's atmosphere, confirming the SOFIA results.*

The timing of this occultation event was also important as it occurred only 15 days before the New Horizons spacecraft's close approach to Pluto. This equates to just 2.5 Pluto days, and thus the SOFIA observations can be considered contemporaneous with the New Horizons data. New Horizons did indeed observe Pluto's atmosphere and confirmed the presence of the haze seen by SOFIA (Figure 20).

FLITECAM data from the Pluto occultation are available (with no flux calibration), from the IRSA archive.

6. REFERENCES

- Bohlin, R. et al. (2014), PASP, 126, 711, doi: 10.1086/677655
- Cohen, M. et al. (2003), AJ, 125, 2645-2663, doi: 10.1086/374362
- Cohen, M. et al. (1999), AJ, 117, 1864, doi: 10.1086/300813
- Croiset, B. et al. 2016, A&A, 590, 26, doi: 10.1051/0004-6361/201527714
- Dehaes, S. et al. (2011), A&A, 533, 17, doi: 10.1051/0004-6361/200912442
- Knight, C. et al. (2021a), ApJ, 918, 8, doi: 10.3847/1538-4357/ac02c6
- Knight, C. et al. (2021b), MNRAS, 509, 3523, doi: 10.1093/mnras/stab3047
- Lord, S. (1992), NASA Technical Memorandum 103957, website: https://ntrs.nasa.gov/citations/19930010877
- McLean, I. et al. (2006), SPIE, 6269, 62695B, doi: 10.1117/12.672173
- Person, M. et al. (2021), Icarus, 356, 113572, doi: 10.1016/j.icarus.2019.113572
- Rayner, J. et al. (2009), ApJS, 185, 289, doi: 10.1088/0067-0049/185/2/289
- Temi, P. et al. (2018), JAI, 7, 1840011-186, doi: 10.1142/S2251171718400111
- Vacca, W. et al. (2015), ApJ, 804, 66, doi: 10.1088/0004-637X/804/1/66

APPENDIX

A. ALL FLOWN FLIGHTS AND TARGETS OBSERVED WITH FLITECAM

Table 8 lists all SOFIA flights where FLITECAM was flown in either the FLITECAM-only or FLIPO configuration and took science and/or engineering data, including commissioning flights.

Table 8: All FLITECAM Flights Flown on SOFIA

Flight Series	Instrument Configuration	Flight Number	Mission ID/Date[1]	Notes
Cycle 1	FLIPO	133	2013-09-27_FP_F133	FLITECAM and HIPO Commissioning[2]
		134	2013-10-01_FP_F134	FLITECAM and HIPO Commissioning[2]
OC2A	FLIPO	144	2014-02-13_FP_F144	Commissioning
		145	2014-02-15_FP_F145	Commissioning
		146	2014-02-19_FP_F146	Partially Commissioning[3]
		147	2014-02-21_FP_F147	Partially Commissioning[3]
		148	2014-02-25_FP_F148	Partially Commissioning[3]
		149	2014-02-27_FP_F149	Partially Commissioning[3]
OCE3	FLIPO	222	2015-06-28_FP_F222	Pluto Occultation rehearsal flight[4]
		223	2015-06-29_FP_F223	Pluto Occultation flight
OC3J	FLITECAM	243	2015-09-29_FC_F243	
		244	2015-10-01_FC_F244	
		245	2015-10-02_FC_F245	
OC4J	FLITECAM	336	2016-10-13_FC_F336	
		337	2016-10-14_FC_F337	
		338	2016-10-15_FC_F338	
		339	2016-10-19_FC_F339	
		340	2016-10-20_FC_F340	
OC5L	FLIPO	436	2017-10-02_FP_F436	Triton Occultation rehearsal/ferry[5] flight
		437	2017-10-04_FP_F437	Triton Occultation rehearsal flight[4]

Flight Series	Instrument Configuration	Flight Number	Mission ID/Date[1]	Notes
		438	2017-10-05_FP_F438	Triton Occultation flight
		439	2017-10-07_FP_F439	

[1]For Mission IDs the numbers preceding "_FP_" are the flight dates, and the numbers after are the flight numbers; [2]Commissioning flights for both FLITECAM and HIPO together in the FLIPO configuration, however no science data were taken; [3]Hybrid commissioning and science flights, some science data were taken on each flight; [4]Mostly or all engineering data taken on these flights; [5]Daytime ferry flight in which some engineering data taken (no science).

Table 9 gives all science targets observed by FLITECAM on SOFIA during its entire operating lifetime. The first column lists the plan ID, which can be utilized in archive searches. The second column is the target name, sometimes edited from the original for clarity. The third column is the principal investigator of the program for which the observations were performed.

Table 9: All Science Targets Observed with FLITECAM

Plan ID	Target	PI
01_0099	HD 189733	Mandell
01_0124	HD 233517	Peeters
02_0015	U Mon	Gehrz
02_0015	V Vul	Gehrz
02_0015	RV Tau	Gehrz
02_0053	GJ 1214	Anderhaus.
02_0056	NGC 7023	Berne
02_0066	16 Psyche	Rivkin
02_0066	2 Pallas	Rivkin
multiple*	SN 2014J	multiple*
03_0020	Nova Sgr 2015 2	Gehrz
03_0024	V605 Aql	Evans
03_0028	Pluto Occultation	Person
multiple*	IRAS 22574+6609	Peeters
03_0032	XX Oph	Peeters
03_0037	HD189733	Swain
03_0042	CoRoT-2	Huber
03_0052	GJ 3470	Angerhaus.

Plan ID	Target	PI
03_0072	StRS 371	Chiar
03_0072	StRS 136	Chiar
03_0084	1 Ceres	Rivkin
03_0084	15 Eunomia	Rivkin
04_0050	44 Nysa	Rivkin
04_0050	22 Kalliope	Rivkin
04_0050	65 Cybele	Rivkin
04_0050	4 Vesta	Rivkin
04_0058	NGC 2023	Tielens
04_0058	Orion	Tielens
05_0180	MACSJ0600.1-1	Egami
70_0003	Orion B	McLean
70_0302	NGC 2024	McLean
70_0402	W3	McLean
70_0402	IRAS 21282+5050	McLean
70_0402	IC 5117	McLean
70_0402	BD +30 3639	McLean
70_0512	Triton Occultation	Dunham
75_0021	S235	Kirsanova
75_0023	Trappist-1	Angerhaus.

** SN 2014J was observed for programs 02_0100, 75_001, and 75_0002 with PIs Garnavich, Hamilton, Gehrz. IRAS 22574+6609 was observed for programs 03_0032 and 04_0112. The first two digits of the Program are the observing Cycle: 70 for Guaranteed Time Observations or 75 for Directors' Discretionary Time.*

Some additional targets that may be useful for science were taken as a part of the FLITECAM commissioning flights. All targets used in these commissioning tests are listed in Table 10. The data for these observations may not be available through the main IRSA archive.

Table 10: Additional Commissioning Targets Observed with FLITECAM

Plan ID	Target
85_0003	M 47
85_0003	HD 73190

Plan ID	Target
85_0003	NGC 2024
85_0003	SA 107-347
85_0003	SA 107-347
85_0003	HD 258439
85_0003	HD 50816
85_0003	HD 29250
85_0004	HD 48481
85_0004	HD 73190
85_0004	HD 200761
85_0004	HD 145454
85_0004	HD 223581

B. ZERO MAGNITUDE FLUXES AND FLUX CALIBRATION FACTORS

The calibration factor derived from standard star observations are summarized in Table 11. The zero magnitude flux values are also given and were based on convolving the filter profiles with a template spectrum of Vega (Cohen et al. 2003). This data can be used to convert from fluxes to magnitudes. The date and instrument configuration are listed for each measurement of the calibration factor. When in the FLIPO configuration, throughput to FLITECAM is slightly lower due to extra optics in the light path.

Table 11. FLITECAM Zero Magnitude Fluxes and Calibration Factors by Filter

Filter Name	Zero Mag. Flux (Jy)	Date	Configuration	CALFCTR (DN/s/Jy)	ERRCALF
FLT_J	1537.7	2/27/14	FLIPO	183074	5%
		10/20/16	FLITECAM	202162	3%
FLT_H	1040.6	2/27/14	FLIPO	212974	5%
		10/20/16	FLITECAM	204476	3%
FLT_Hwide	889.9	10/7/17	FLIPO	303986	3%
FLT_Pa	721.0	2/27/14	FLIPO	10311	5%
		10/2/15	FLITECAM	12924	6%
		10/20/16	FLITECAM	10407	3%
		10/7/17	FLIPO	9726	3%
FLT_Pa_Cont	814.7	2/27/14	FLIPO	10301	5%
		10/2/15	FLITECAM	12589	6%
		10/20/16	FLITECAM	10238	3%
		10/7/17	FLIPO	9043	3%
FLT_K	682.0	2/27/14	FLIPO	130563	5%
		10/20/16	FLITECAM	150396	3%
		10/7/17	FLIPO	119448	3%
FLT_ICE_308	351.4	2/27/14	FLIPO	34597	5%
		10/2/15	FLITECAM	32017	6%
		10/20/16	FLITECAM	38634	3%
		10/7/17	FLIPO	31685	3%
FLT_PAH_329	290.2	2/27/14	FLIPO	20104	5%
		10/2/15	FLITECAM	19755	6%
		10/20/16	FLITECAM	22878	3%

Filter Name	Zero Mag. Flux (Jy)	Date	Configuration	CALFCTR (DN/s/Jy)	ERRCALF
		10/7/17	FLIPO	17912	4%
FLT_L	272.7	10/20/16	FLITECAM	206047	3%
FLT_NbL	262.0	2/27/14	FLIPO	44773	5%
		10/20/16	FLITECAM	46458	4%
FLT_Lprime	232.7	10/20/16	FLITECAM	208552	3%

C. FLITECAM FILTER WAVELENGTHS

In Table 12, each FLITECAM filter is given with an approximate central reference wavelength. Also given are the mean and pivot wavelength values (Bohlin et al. 2014) for each filter, whose uses are discussed in Sections 4.4.1 and 4.4.1.1. As these depend on whether FLITECAM was being used in the FLIPO or FLITECAM-only configuration, two sets of values are given.

Table 12: Mean and Pivot Wavelengths for FLITECAM Filters

Filter	λ_{ref} (μm)	FLITECAM-only		FLIPO	
		λ_{mean} (μm)	λ_{pivot} (μm)	λ_{mean} (μm)	λ_{pivot} (μm)
J	1.2500	1.2416	1.2391	1.2464	1.2440
H	1.6500	1.6316	1.6296	1.6322	1.6302
H_{wide}	1.8000	1.7932	1.7867	1.7941	1.7877
K	2.1200	2.1051	2.1025	2.1058	2.1033
K_{long}	2.5000	2.4852	2.4818	2.4855	2.4822
K_{wide}	2.3200	2.3080	2.2972	2.3102	2.2994
L	3.5500	3.5346	3.5308	3.5347	3.5308
L′	3.8700	3.8480	3.8443	3.8486	3.8450
L+M	4.1000	4.0874	4.0104	4.0921	4.0153
M	4.9000	4.8438	4.8413	4.8438	4.8413
L_{narrow}	3.6100	3.6027	3.6023	3.6027	3.6023
M_{narrow}	4.8100	4.8066	4.8063	4.8066	4.8063
H_2O Ice	3.0500	3.0502	3.0498	3.0502	3.0499
Paschen α	1.8700	1.8743	1.8743	1.8743	1.8743
Pa α Continuum	1.9000	1.9001	1.9001	1.9001	1.9001
Pa α + H_{wide}	1.8700	1.8744	1.8743	1.8744	1.8743
Pa α Cont + H_{wide}	1.9000	1.9001	1.9000	1.9001	1.9000
PAH	3.3000	3.3006	3.3005	3.3007	3.3006

Note: λ_{ref} is the reference wavelength of the filter. Bandwidths for each filter are given in Table 2.

D. IMPORTANT FLITECAM HEADER KEYWORDS

Some of the more important header entries for FLITECAM are explained below. The common values the header keywords have for science data are also provided. Other values may be possible, but only in engineering data. Review of other general keywords in the header that are not specific to FLITECAM or not covered below are in the *SOFIA FITS Keyword Dictionary* available at the IRSA SOFIA Data Processing website. Common standardized FITS header information like WCS information are not described here.

Since the information in the FLITECAM headers is not organized in any systemic fashion, the header information below is divided into major groupings used by the Data Cycle System (DCS).

--- DCS DATA COLLECTION ---		
FITS Keyword	Value	Description
CHOPPING	T/F	Should always be F (FLITECAM did not utilize the telescope's chopping functionality)
NODDING	T/F	T if telescope was nodding during observation
DITHER	T/F	T if telescope was dithering during observation
MAPPING	T/F	Should always be F (FLITECAM did not utilize the telescope's default mapping functionality)
SCANNING	T/F	Should always be F (FLITECAM did not utilize the telescope's default scanning functionality)
--- DCS INSTRUMENT ---		
FITS Keyword	Value	Description
DATATYPE	IMAGE SPECTRAL OTHER	IMAGE for imaging observations, SPECTRAL for grism observations. Other may include special modes.
INSTCFG	IMAGING GRISM SPECTROSCOPY	FLITECAM instrument configuration.
INSTMODE	STARE NOD_OFFARRAY NOD_ALONG_SLIT NOD_OFF_SLIT	Mode of data collection. See Section 2.3 for descriptions.

EXPTIME	[FLOAT]	Total file integration time. This is the time that should be used for science. Equals INTTIME*NEXP*CYCLES
CYCLES	[INT]	Number of times observations are cycled
NEXP	[FLOAT]	Nominal number of coadded exposures
INTTIME	[FLOAT]	On-source integration time per coadded exposure in seconds. Equals ITIME*COADDS
ITIME	[FLOAT]	Integration time for a single frame readout in seconds
COADDS	[INT]	Number of coadded frames used
SPECTEL1	NONE FLT_DRK FLT_J FLT_H FLT_K FLT_ICE_308 FLT_PAH_329 FLT_Pa FLT_Pa_cont FLT_NbL FLT_NbM FLT_L FLT_Lprime FLT_M FLT_B3_J FLT_C4_H FLT_A3_Hw FLT_B2_Hw FLT_C3_Kw FLT_A2_KL FLT_C2_LM FLT_B1_LM FLT_A1_LM	Filter or grism present during observation
SPECTEL2	NONE FLT_SS10 FLT_SS20	Spectroscopic slit present during observation (redundant with SLIT)
WAVECENT	[FLOAT]	Calculated mean wavelength of the filter or grism based upon instrument throughput

--- DCS ARRAY DETECTOR ---		
FITS Keyword	Value	Description
DETECTOR	SBRC InSb	FLITECAM Detector type
PIXSCAL2	[FLOAT]	The pixel scale for FLITECAM should always be 0.475 arcseconds per pixel
SATURATE	[INT]	Count value at which the data begin to saturate
ARRAY0	[STRING]	If the data is being readout in a subarray, this string will give its location offset (x, y) from array center and subarray dimensions in the following format [x, y, width, height]
--- DCS NODDING ---		
FITS Keyword	Value	Description
NODTIME	[FLOAT]	Integration time at each nod position in seconds.
NODAMP	[FLOAT]	Total distance telescope nodded in arcsec (aka “nod throw” since it is not really an amplitude)
NODBEAM	A B	Nod beam position
NODPATT	AB ABBA	Nod cycle pattern between the two nod positions, A and B.
NODCRSYS	ERF SIRF	This is the coordinate system the nodding is being defined in: ERF is the Equatorial Reference Frame (aka Sky coordinates) and SIRF is the Science Instrument Reference Frame (aka Array coordinates)
NODANGLE	[FLOAT]	Actual nod angle in degrees in the NODCRSYS coordinate system measured by telescope encoders
--- DCS DITHERING ---		
FITS Keyword	Value	Description
DTHNPOS	[INT]	Number of dither positions used to create the final image

DTHPATT	NONE 3-POINT 5-POINT 9-POINT CUSTOM	Dither pattern used for observations
DTHOFFS	[FLOAT]	Dither offset value in arcseconds
DTHCRSYS	ERF SIRF	This is the coordinate system the dithering is being defined in: ERF is the Equatorial Reference Frame (aka Sky coordinates) and SIRF is the Science Instrument Reference Frame (aka Array coordinates)
--- NON-DCS —		
FITS Keyword	Value	Description
TRACKING	T/F	T means that guiding (tracking) was on during observation.
ROT_ANGL	[FLOAT]	Direction the y-axis of the FLITECAM array (i.e. “up”) is oriented with respect to North on the sky (redundant with TELVPA)
TELVPA	[FLOAT]	Direction the y-axis of the FLITECAM array (i.e. “up”) is oriented with respect to North on the sky (redundant with ROT_ANGL)
ZA_START	[FLOAT]	Zenith angle at the start of the observations
ZA_END	[FLOAT]	Zenith angle at the end of the observations
--- PIPELINE RELATED KEYWORDS (IMAGING) —		
FITS Keyword	Value	Description
ASSC_AOR	STRING	All AOR-IDs used in making the data
CALFCTR	[FLOAT]	Calibration factor (counts/s/Jy), same as the “reference calibration factor” given in the HISTORY section of the header. Used as a divider for COA imaging files to convert to CAL files.
ERRCALF	[FLOAT]	Calibration factor uncertainty (counts/s/Jy)

LAMREF	[FLOAT]	Reference wavelength (microns), as given in Table 12.
BUNIT	[String]	The units of the pixels in the final data. For imaging this will be Jy.
--- PIPELINE RELATED KEYWORDS (GRISM) —		
FITS Keyword	Value	Description
SLIT	NONE FLT_SS10 FLT_SS20	Spectroscopic slit present during observation (redundant with SPECTEL2)
SLTH_ARC	[FLOAT]	Slit height on sky in arcsec
SLTH_PIX	[FLOAT]	Slit height on array in pixels
SLTW_ARC	[FLOAT]	Slit width on sky in arcsec
SLTW_PIX	[FLOAT]	Slit width on array in pixels
RP	[FLOAT]	Resolving power of grism and slit being used
APPOSO01	[FLOAT]	Aperture centroid measured in arcsec used to extract the spectrum.
NAPS	[INT]	Number of apertures used
ORDERS	STRING	Order numbers
RP	[INT]	Resolving power
APRADO01	[FLOAT]	Extraction aperture radii in arcsec
BGR	STRING	Location of the regions used for background subtraction
BGORDER	[INT]	Background polynomial fit degree
WAVECAL	STRING	Filename identifying the wavelength calibration map used to calibrate the data.
DISPO01	[FLOAT]	Dispersion in microns per pixel of data
LINEFILE	STRING	Filename identifying the linearity coefficients applied

WAVSHIFT	FLOAT	Wavelength shift used to shift the MRG file compared to the ATRAN model for optimal telluric subtraction.
XUNITS	STRING	Units of the wavelength axis e.g., μm
YUNITS	STRING	Units of the spatial axis e.g., arcsec

B1. HISTORY Section of Imaging Headers

Below is an example of selected parts of the HISTORY section at the bottom of the FLITECAM imaging headers containing information that may be of importance or require further explanation. This section of the FITS headers is annotated with explanations.

```
HISTORY MODULE = FDRP_TellCorr
HISTORY Using reference files:
HISTORY   flitecam/response/rfit_am_noflipo_20140227.txt
HISTORY   flitecam/response/rfit_alt_noflipo_20140227.txt
HISTORY Reference ZA=45, altitude=41
HISTORY Telluric correction factor to ZA=51.6153, altitude=42.9940:
HISTORY   1.0012523

HISTORY    Data planes are:
HISTORY      1. Image
HISTORY      2. Uncertainty
HISTORY      3. Bad pixel mask (0=good, 1=bad)
HISTORY      4. Exposure map

HISTORY MODULE = FluxCal Update
HISTORY Applying cal factor from table to data and header in CAL file
HISTORY
HISTORY Flux calibration information:
HISTORY Using reference file:
HISTORY   flitecam/ref_calfctr/refcalfac_20171007_v1.txt
HISTORY Average reference calibration factor:
HISTORY   20104.620 +/- 936.81000
HISTORY Data divided by cal factor to convert from DN/sec to Jy

HISTORY Notes from quality analysis
HISTORY ---------------------------
HISTORY These observations contains two dithered set, users are advised
HISTORY to coadd these data to get higher SNR product. Artifact due to
HISTORY debris on the entrance window is seen in the data. Setting
HISTORY DATAQUAL to USABLE. Data is reprocessed due to availability of
HISTORY updated reference calibration values.
HISTORY
HISTORY   DATAQUAL: GOOD -> USABLE
HISTORY   WCSQUAL: None -> NOMINAL
HISTORY   CALQUAL: None -> NOMINAL
```

< Telluric correction factor applied and reference files used.

< Description of the data FITS planes content.

< This section shows that flux calibration was applied to the data.

< Flux cal factor applied to data to convert from DN/sec (or ct/sec) to Jy.

< This section has detailed notes of any problems with the data. Refer to the descriptions of Known Issues in Section 4.1.

< Final assessment of data quality and calibration quality

B2. HISTORY Section of Grism Headers

Below is an example of selected parts of the HISTORY section at the bottom of the FLITECAM headers with specific information that may be of importance for grism data. This section requires little additional annotation/explanation as it is quite verbose in describing the data used and the reduction processes to create the FITS data.

```
HISTORY FSpextool History

HISTORY Description of reduction:
HISTORY This image was created by subtracting Oct_15_2016_0391.a.fits
HISTORY from Oct_15_2016_0390.a.fits.  The raw data was corrected for
HISTORY non-linearity using the coefficients file
HISTORY lc_coeffs_20140325.fits.  In the 3-D array, the first plane is
HISTORY the data array.  That is, data = array[*,*,0].  The next plane
HISTORY is the variance array (var = array[*,*,1]).
HISTORY
HISTORY ------------------------------------------------------------
HISTORY
HISTORY FSpextool History
HISTORY -----------------
HISTORY
HISTORY Input ObsIDs: 161015_000_00FL0390
HISTORY
HISTORY Description of reduction:
HISTORY This spectrum was extracted from
HISTORY F0338_FC_GRI_0401126_FLTB1LMFLTSS20_IMG_0390-0391.fits.  The
HISTORY image was corrected for non-linearity using coefficients file
HISTORY lc_coeffs_20140325.fits.  The flat flat_lmb_multinight.fits was
HISTORY used to find the edges of the order in the extraction process.
HISTORY The image and flat were used to define smoothed spatial
HISTORY profiles.  These profiles were used to determine aperture
HISTORY centers and radii.  Background regions were determined, fit, and
HISTORY subtracted from the spectra during extraction.  The wavecal file
HISTORY lmb_map_arcs.fits was used to determine the wavelength
HISTORY calibration.  The spectra were extracted using standard
HISTORY extraction.  Bad pixels were fixed during extraction, including
HISTORY pixels above saturation level 5000 in the raw image.
HISTORY
HISTORY Description of data:
HISTORY The output FITS files contain a 3-D array of data consisting of
HISTORY sets of triplet arrays of data for each aperture and each order,
HISTORY where each triplet is composed of an array for the wavelength,
HISTORY an array for the flux, and an array for the error. The triplets
HISTORY for each aperture are stacked behind one another, followed by
HISTORY the triplets for the next order, etc. If no orders have been
HISTORY skipped or deselected in the extraction process, the contents of
HISTORY aperture Y in order X can be found as follows:lambda =
HISTORY array[*,0,( X - (smallest order number))*naps + (Y-1)], flux   =
HISTORY array[*,1,( X - (smallest order number))*naps + (Y-1)], error  =
HISTORY array[*,2,( X - (smallest order number))*naps + (Y-1)]  For
HISTORY example, for an SXD file with two apertures, the wavelength
HISTORY array for aperture 1 in order 3 is located in array [*,0,0], the
HISTORY flux is in array [*,1,0] and the error is in array [*,2,0]. For
HISTORY aperture 2, the wavelength is in array [*,0,1], the flux is in
```

< Overview of reduction.

< Detailed description of reduction.

< Description of the data in this FITS file.

```
HISTORY array [*,1,1] and the error is in array [*,2,1]. For order 4,
HISTORY the flux for aperture 1 is in array [*,1,2], while the flux for
HISTORY aperture 2 is in array [*,1,3]. For order 5, the fluxes for the
HISTORY two apertures are in arrays [*,1,4] and [*,1,5], etc.
HISTORY
HISTORY Additional processing:
HISTORY The spectra were shifted in wavelength by 0.00000 pixels to
HISTORY match the atmospheric model.The spectra were calibrated by
HISTORY dividing by the atmospheric transmission model
HISTORY (atran_43K_45deg_1-6mum.fits) and the instrumental response
HISTORY (FC_GRI_B1LM_SS20_RSP.fits). These models are recorded in the
HISTORY spectra as columns 4 and 5, respectively.
HISTORY
HISTORY ------------------------------------------------------------
HISTORY
HISTORY Headers updated by dsandel, 2016-11-21T14:13:54
HISTORY   CALQUAL: None -> NOMINAL
HISTORY   WCSQUAL: None -> NOMINAL
HISTORY   DATAQUAL: None -> NOMINAL
```

< Final assessment of data quality and calibration quality.